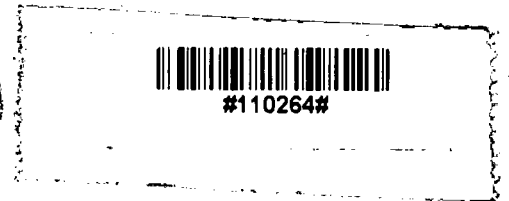
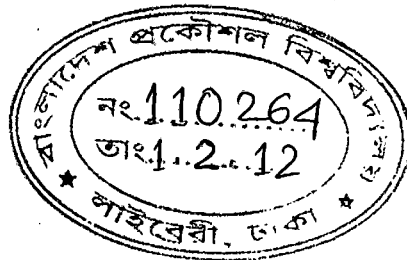


INVESTIGATION OF THE MECHANICAL AND ELECTRICAL
PROPERTIES OF POLYPROPYLENE-TITANIUM OXIDE COMPOSITES

Sharmin Seema
Roll No. 040514017
Session: April 2005



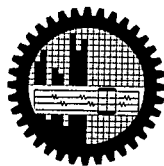
BUET

Department of Physics,
Bangladesh University of Engineering and Technology (BUET)
Dhaka 1000
September 2010.

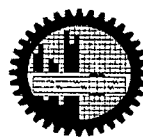
**INVESTIGATION OF THE MECHANICAL AND ELECTRICAL
PROPERTIES OF POLYPROPYLENE-TITANIUM OXIDE COMPOSITES**

A dissertation submitted to the Department of Physics, Bangladesh University of Engineering and Technology (BUET) in partial fulfillment of the requirement for the degree of Master of Philosophy (M. Phil.) in Physics.

By
Sharmin Seema
Roll No. 040514017
Session: April 2005







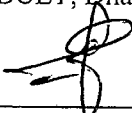
Department of Physics,
Bangladesh University of Engineering and Technology (BUET)
Dhaka 1000
September 2010.



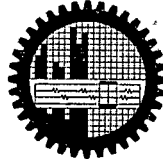
Certification of Thesis Work

The thesis titled "INVESTIGATION OF THE MECHANICAL AND ELECTRICAL PROPERTIES OF POLYPROPYLENE TITANIUM OXIDE COMPOSITES" submitted by SHARMIN SEEMA Roll No- 040514017P, Registration No. 040514017, Session: April/2005 has been accepted as satisfactory in partial fulfillment of the requirement for the degree of Master of Philosophy (M. Phil.) in Physics on 29 September, 2010.

BOARD OF EXAMINERS

1. 
DR. MD. ABU HASHAN BHUIYAN (Supervisor) Chairman
Professor
Department of Physics
BUET, Dhaka-1000
2. 
DR. A. K. M. AKTHER HOSSAIN (Ex-Officio) Member
Professor & Head
Department of Physics
BUET, Dhaka-1000
3. 
DR. NAZMA ZAMAN Member
Professor
Department of Physics
BUET, Dhaka-1000
4. 
DR. MD. FORHAD MINA Member
Associate Professor
Department of Physics
BUET, Dhaka-1000
5. 
DR. M. A. GAFUR Member (External)
Senior Engineer
Bangladesh Council for Scientific and Industrial Research
(BCSIR), Dhaka

Bangladesh Council for scientific and industrial research
(BCSIR), Dhaka.



BUET

CANDIDATE'S DECLARATION

I is hereby declared that this thesis or any part of it has not been submitted elsewhere for
the award of any degree or diploma.

Sharmin Seema
(Sharmin Seema)
Roll No. 040514017
Session: April 2005

Dedicated to
My beloved Mother and Father

CHAPTER 1	INTRODUCTION	
1.1 Introduction		2
1.2 Review of Earlier Research Works		2
1.3 Objectives		9
1.4 Thesis Layout		10
CHAPTER 2	FUNDAMENTAL ASPECTS OF POLYMER, POLYPROPYLENE, TITANIUM DIOXIDE AND COMPOSITES	
2.1 Polymers		
2.1.1 Definition of Polymer		12
2.1.2 Classification of Polymers		12
2.2 Polypropylene		14
2.2.1 Chemical and Physical Properties of Polypropylene		15
2.2.2 Electrical Properties		17
2.2.3 Mechanical Properties		17
2.2.4 Thermodynamic Properties		18
2.2.5 Application of Polypropylene		19
2.3 Titanium dioxide		21
2.3.1 Physical and Chemical Characteristics		22
2.3.2 Applications of TiO ₂		23
2.4 Composites		
2.4.1 Definition		25

2.4.2 Different types of Composite Materials	26
2.5 Theory of Mechanical Properties of Composites	
2.5.1 Concepts of stress and strain	28
2.5.2 Stress-strain behavior	30
2.5.3 Anelasticity	32
2.5.4 Tensile properties	33
2.5.5 True stress and strain	33
2.5.6 Elongation	33
2.5.7 Hardness	34
2.6 Thermal Analysis	
2.6.1 Theory of thermal analysis	34
2.6.2 Differential thermal analysis	34
2.6.3 Thermogravimetric analysis	37
2.6.4 Differential scanning calorimetry	38
2.6.5 Scanning electron microscopy	39
2.7 Dielectrics	40
2.7.1 Dielectric constant	41
2.7.2 Dielectric loss	41
2.7.3 Debye relaxation	42
CHAPTER 3	EXPERIMENTAL DETAILS
3.1 Raw Materials	44
3.2 Equipment for Sample Preparation	44
3.2.1 Fabricated extrusion machine	44
3.3 Composite Preparation Procedure	46
3.4 Mechanical Testing	46

3.5 Scanning Electron Microscopy	47
3.6 Methods of Measuring Mechanical Properties	47
3.6.1 Tensile Test	48
3.6.2 Micromechanical testing	48
3.7 Thermal Testing	49
3.8 AC Electrical Measurements	49
3.8.1 Instruments	49
3.8.2 AC measurement procedure	52

CHAPTER 4 RESULTS AND DISCUSSION

4.1 Surface morphology	56
4.2 Mechanical properties	59
4.3 Micromechanical properties	61
4.4 Thermal Analyses	62
4.5 AC electrical Studies	
4.5.1 Variation of AC conductivity on frequency at different temperatures	65
4.5.2 Dependence of dielectric constants on frequency at different temperatures	67
4.5.3 Variation of loss tangent with frequency and temperature	70

CHAPTER 5 CONCLUSIONS

5.1 Conclusions	77
5.2 Suggestions for future work	77
5.3 References	78

LIST OF FIGURES

Chapter 2

Figure 2.1: Polypropylene

Figure 2.2: The true stress-true strain curve

Figure 2.3: Extension of a spring

Figure 2.4: Schematic illustration of a DTA cell.

Chapter 3

Figure 3.1: The Extrusion Machine setup in the laboratory

Figure 3.2: Hounsfield Universal Testing Machine (UTM)

Figure 3.3: Different views of the tensile test specimen

Figure 3.4 Arrangement of AC measurement

Figure 3.5: Photograph of oil rotary pump

Figure 3.6: Photograph of the specimen holder

Chapter 4

Figure 4.1 SEM micrographs of the (a) iPP sample, (b) 10 (c) 20 (d) 30 and (e) 40 wt% TiO₂ loaded composites after fracture through the tensile test

Figure 4.2: SEM micrographs of the extrusion-molded samples [(a)–(c)] and the extrusion cum compression-molded samples [(d)–(f)]: (a) and (d) neat iPP, (b) and (e) iPP þ 20 wt% TiO₂ and (c) and (f) iPP þ 40 wt% TiO₂.

Figure 4.3: Tensile stress versus strain of the neat sample and composites with various concentrations of TiO₂ (A: neat iPP, B: 10% wt% TiO₂, C: 20% wt% TiO₂, D: 30% wt% TiO₂, E: 40% wt% TiO₂, F: 50% wt% TiO₂)

Figure 4.4: Variation of tensile strength and elongation-at- break (%) of the iPP/TiO₂ composites with increasing filler content

Figure 4.5: Change of microhardness at various concentrations of filler for both extrusion molded and extrusion cum compression molded samples

Figure 4.6(a): DTA thermograms of the extrusion cum compression molded neat iPP sample and iPP/TiO₂ composites having various contents of TiO₂.

Figure 4.6(b): TGA thermograms of the extrusion cum compression molded neat iPP

sample and iPP/TiO₂ composites having various contents of TiO₂.

Figure 4.7: DSC curves showing the glass transition temperatures of the composites with different filler concentrations

Figure 4.8 (a) Dependence of ac conductivity on frequency for iPP/TiO₂ composite with 10% TiO₂ at different temperatures

Figure 4.8 (b) Dependence of ac conductivity on frequency for iPP/TiO₂ composite with 20% TiO₂ at different temperatures

Figure 4.8 (c) Dependence of ac conductivity on frequency for iPP/TiO₂ composite with 30% TiO₂ at different temperatures

Figure 4.8 (d): Dependence of ac conductivity on frequency for iPP/TiO₂ composite with 50% TiO₂ at different temperatures

Figure 4.9 (a) Variation of dielectric constant with frequency for iPP/TiO₂ composite with 10 % TiO₂ at different temperatures

Figure 4.9 (b) Variation of dielectric constant with frequency for iPP/TiO₂ composite with 20 % TiO₂ at different temperatures

Figure 4.9 (c) Variation of dielectric constant with frequency for iPP/TiO₂ composite with 30 % TiO₂ at different temperatures

Figure 4.9(d) Variation of dielectric constant with frequency for iPP/TiO₂ composite with 40 % TiO₂ at different temperatures

Figure 4.9(e) Variation of dielectric constant with frequency for iPP/TiO₂ composite with 50 % TiO₂ at different temperatures

Figure 4.10 (a) Variation of loss tangent with frequency at different temperatures for iPP/TiO₂ composite with 10 wt % of TiO₂

Figure 4.10 (b) Variation of loss tangent with frequency at different temperatures for iPP/TiO₂ composite with 20 wt % of TiO₂.

Figure 4.10 (c) Variation of loss tangent with frequency at different temperatures for iPP/TiO₂ composite with 30 wt % of TiO₂

Figure 4.10 (d) Variation of loss tangent with frequency at different temperatures for iPP/TiO₂ composite with 40 wt % of TiO₂.

Figure 4.10 (e) Variation of loss tangent with frequency at different temperatures for iPP/TiO₂ composite with 50 wt % of TiO₂.

LIST OF TABLES

Chapter 2

Table 2.1: Electrical Properties of iPP-TiO₂

Table 2.2: Mechanical properties of iPP-TiO₂

Chapter 4

Table 4.1: Melting and degradation temperatures (T_m and T_d) and resistivity measured at 30 °C for both extrusion-molded and extrusion cum compression-molded samples

Acknowledgements

At first for constant blessings upon 'Allah' I am most grateful that I able to complete my thesis work.

I put forth my gratefulness to Bangladesh University of Engineering and Technology (BUET) for providing me financial and full support for my thesis work.

Here I deliver my sincere gratitude and respect to Dr. Md. Abu Hashan Bhuiyan, Professor, Department of physics, BUET for letting me to do my research work. I am very grateful and honored to get his constant kind supervision, inspiration, important suggestions, and guidance, about the research work and for showing me the way to advanced research.

I am also expressing my heartiest gratitude and respect to Prof. Dr. A. K. M. Akther Hossain, Head, Dept. of physics. I am grateful to Prof. Dr. Nazma Zaman, Prof. Dr. Jiban Podder, Prof. Dr. Md. Feroz Alam Khan, Mrs. Fahima Khanam, Dr. Md. Mostak Hossain, Dr. Md. Forhad Mina, for providing all research facilities available in the Department and for giving me full mental support and encouragement in finishing my thesis work.

I am also expressing my respect and heartiest gratitude to

- Dr. Afia Begum, Dr. Md. Rafi Uddin, Assistant Prof. Department of Physics, (BUET)

Lecturers of Department of Physics - Muhammed Samir Ullah, Mohammed Jellur Rahman, Mohammed Abu Sayem Karal.

- Mr. Yousuf Khan, Instrument Engineer, Dept. of Material and Matalurgy.
- Mr. Rama Bijoy Sharker, Mr. Sunirmal Majumder, Mr. Mostofa Kamal, Mr. Ali Ashraf, Ms. Nasima Banu, Ms. Rummana Matin and Ms. Happy Day.- Students, Dept. of Physics (BUET).

I am also grateful to all the staff members of department of physics BUET for there full cooperation.

My thanks giving go to the authority of BCSIR, Dhaka for allowing me to perform my mechanical research and thermal test in their laboratories.

Finally I wish to convey my gratitude to all of my family members.

ABSTRACT

Titanium dioxide (TiO_2)-filled isotactic polypropylene (iPP) composites with various contents of TiO_2 were prepared by a locally fabricated extrusion molding machine. The extrudates were melt-pressed at 180°C and produced as plane sheets of nearly equal thickness by rapid cooling.

The iPP sample shows the smoothest surface in comparison to other two composites, and the composite surface of 20 wt% TiO_2 seems to be slightly smoother and becomes less white than that of 40 wt% filler. The composite of 40 wt% TiO_2 contains more agglomerates or larger particles, which seem to form lumps on the surface, than the composite of 20 wt% TiO_2 . Increasing TiO_2 content develops slight roughness and whiteness on the ECM composite surfaces but does not show any noticeable gap or sharp boundary between filler and polymer matrix. Gaps are significantly notable in the EM composite of 40 wt% TiO_2 . Small particles are seen to disperse inhomogeneously in the iPP matrix in the composite samples. While the surface of the neat iPP shows a few cracks, terraces and voids, a considerable amount of voids appear in the composites indicating different fracture processes in the neat iPP and the composites.

Scanning electron micrographs taken on the fractured surface of the samples show increasing amount of voids with increasing filler content. Tensile strength, elongation-at-break (%) and glass transition temperature of the samples are found to decrease considerably with the increase in TiO_2 content, whereas microhardness decreases slightly with the filler content. The thermal behavior of iPP- TiO_2 composites was analyzed by thermogravimetric, differential thermal analyses and differential scanning calorimetry. It is seen that the melting temperature does not show any noticeable change but the degradation temperature increases with the increase of filler. Glass transition temperature decreases as TiO_2 content increases in the composites.

It is observed that the ac conductivity increases with the increase of frequency but very weakly dependent on temperature. The dielectric constant decreases with the increase in frequency and not much dependent on temperature. As the frequency increases the dipoles in the composite can not follow the field and thus lag behind the applied field. So

the value of the dielectric constant decreases with the increase of frequency. As the frequency increases the loss tangent increases and at a particular frequency the loss tangent attains a maximum value. After reaching the maximum, the loss tangent decreases with the increase in frequency. It is also observed that for a particular frequency, the loss tangent is higher at higher temperature. This low frequency relaxation peak indicates that the dielectric loss may be due to interfacial propagation in these composites.

Sharmin Seema
Student : M.Phil
Roll:040514017P
Session: April 2005

Acknowledgements

Regarding the outcome of this thesis, I express my deepest sense of gratitude, indebtedness and deep appreciation to my respected supervisor Professor Dr. Md. Abu Hashan Bhuiyan, Department of Physics, Bangladesh University of Engineering & Technology, (BUET) Dhaka, for his continuous personal care, close supervision, constant inspiration, helpful attitude, effective suggestions throughout the long period of my research work and also for acquainting me with the advanced world.

I am highly grateful to respectable members of the Doctoral Committee Prof. Dr. A. K. M. Akther Hossain, Professor Dr. Mominul Huq, Professor Dr. Jiban Podder, Prof. Dr. Md. Feroz Alam Khan, Department of Physics, BUET and Professor Dr. Md. Mohar Ali, Materials science and Metallurgical Engineering, BUET.

I am deeply indebted to the Head and my respected teachers Prof. Dr. Nazma Zaman, Prof., Ms. Fahima Khanam, Dr. Md. Forhad Mina, all the teachers of the Department of Physics, BUET for providing necessary facilities, also for their inspiration, affection and constructive suggestions throughout the long road of research. I would like to express my sincere thanks particularly to Mr. Md. Jellur Rahman, lecturer, Department of Physics, BUET for his fulltime cooperation. The encouragement and cooperation I received from Mr. Rama Bijoy Sarker, are greatly acknowledged. I would like to extend my thanks to all other Ph. D and M. Phil students of the Department, BUET for scientific discussions and making this department a pleasant and friendly working place.

I would like to thank all the staff members of this Department specially Mr. Md. Idris Munshi, Mr. Liakot Ali, Mr. Swapan Kumar Das for their sincere help to do this research work. Thanks are directed to all my friends who showed an interest in my work.

Finally, I would like to express my heartfelt obligation thanks to my parents, brothers, sister and all others family members for their multifaceted support.

I acknowledge the financial support offered by the authority of Bangladesh University of Engineering and Technology (BUET).

Chapter 3

Table 3.1 Physical properties of vinylene carbonate (C₃H₂O₃)

Chapter 4

Table 4.1: Composition of elements in PPVC thin films.

Table 4.2 Some Characteristics bonds and their corresponding peaks in the IR spectra.

Table-4.3 Assignments of FTIR absorption bands for VC, PPVC and PPVC.

Chapter 5

Table-5.1 Wavelength corresponding to maximum absorbance of PPVC thin films for various thicknesses.

Table-5.2: Direct energy band gap for different thicknesses at room temperatures

Table-5.3 Maximum absorbance to corresponding wavelength for samples of different thicknesses at different temperatures.

Table-5.4 Direct energy band gap for as deposited and heat treated PPVC thin films of different thicknesses

Chapter 6

Table-1 Values of ‘n’ at different temperatures for PPVC samples

Table-2 Comparison between the theoretical and experimental β coefficients (100 nm)

Table-3 Comparison between the theoretical and experimental β coefficients (130 nm)

Table-4 Comparison between the theoretical and experimental β coefficients (150 nm)

Table-5 Comparison between the theoretical and experimental β coefficients (200 nm)

Chapter 7

Table 7.1 The values of the exponent “n” at different temperatures

Abbreviations and symbols

ABS	Absorbance
AC/ac	Alternating Current
Al	Aluminium
B	Tauc Parameter
Cr-Al	Chromel -Alumel
CC/cc	Capacitively Coupled
d	Thickness
DC/dc	Direct Current
DTA-	Differential thermal analysis .
EA	Elemental Analysis
FL	Fermi Level
FTIR--	Fourier Transform Infrared Spectroscopy
	Current
I	
<i>I</i>	Intensity of Radiation
IR	Infrared
J	Current density
k	Boltzmann Constant
K	Extinction Co-efficient
LB	Langmuir-Blodgett
MHz	Mega Hertz
PECVD	Plasma Enhanced chemical Vapour Deposition.
PVD	Physical Vapour Deposition.
PF	Poole-Frenkel
PPVC	Plasma Polymerized Vinylene Carbonate.
PPDP	Plasma Polymerized Diphenyl.
PPm-X	Plasma Polymerized m-Xylene
PPPA	Plasma Polymerized Polyaniline
RF/rf	Radio Frequency
SCLC	Space Charge Limited Current.
UV-	Ultra- Violet
SEM-	Scanning Electron Microscopy.
TGA-	Thermogravimetric Analysis.

CANDIDATE'S DECLARATION

It is hereby declared that this thesis or any part of it has not been submitted elsewhere for the award of any degree or diploma.

CHAPTER 1

INTRODUCTION

1.1 Introduction	2
1.2 Review of Earlier Research Works	2
1.3 Objectives	9
1.4 Thesis Layout	10

1.1 Introduction

Isotactic polypropylene (iPP) is a highly crystallizable, low cost, balance-strength and widely used thermoplastic in automotive industries. However its use in the production of newly emerging materials, such as composites and blends, where filler plays potential role in controlling their properties, is progressively expanding to meet engineering requirements. Filler-reinforced polymer composites have gained much attention to scientific investigations in recent years, because the incorporation of fillers alters the structural, mechanical, thermal and electrical properties of the composite materials [1-5]. These properties are affected by the degree of dispersion of filler into the polymer matrix and the interaction between filler and polymer [2]. In this context, inorganic fillers play important role in changing thermal, mechanical and electrical properties [2-7]. Commonly used fillers in iPP are talc, calcium and clay [1, 5] but titanium dioxide (TiO₂) can be one of the important fillers in producing composites with improved properties [2]. Due to practical and technological importance of composites, we have focused our interest in synthesizing iPP/TiO₂ composites in order to investigate their structural, micromechanical, thermal and electrical properties for understanding the influence of TiO₂ and processing conditions on the final products. These findings can provide valuable scientific information about the mechanisms of filler dispersion into the iPP matrix, the effect of fillers and processing routes on the aforesaid various properties.

1.1 Review of earlier research works

Recently, researchers are much interested to do research on polymer composites because mixing different types of material with polymer, the mechanical, electrical, and thermal properties of composites are changed. Polymers offer many advantages over conventional materials including lightness, resilience to corrosion and ease of processing. They can be combined with fibers to form composites which have enhanced properties, enabling them to be used as structural members and units. Polymer composites can be used in many different forms ranging from structural composites in the construction industry to the high technology composites of the aerospace and space satellite industries.

Semko et al. [8] investigated the effect of TiO₂ nanoparticles on the resistivity and gas-sensing performance of Poly(vinylchloride)-expanded graphite composites. Composites

of poly(vinyl chloride) (PVC) and TiO₂-modified expanded graphite (EG) have been prepared, with TiO₂ contents on the EG surface from 0 to 20 wt % and EG contents from 0 to 100%, and their structural, electrical, and gas-sensing properties have been studied. The results demonstrate that by varying the composition of the composites, one can control their percolation threshold, electrical properties, and gassensing performance. The objective of this work was to study the effect of nanocrystalline titania particles on the electrical and gas-sensing properties of PVC–EG composites. The present results may be useful in designing advanced materials for gas detection.

Hui et al. [9] studied the influence of surface-modified TiO₂ nanoparticles on fracture behavior of injection molded polypropylene(PP). The transmission electron microscopy (TEM) and scanning electron microscopy (SEM) images showed homogeneous dispersion of nano-TiO₂ at 1 vol.% filler content and weak nanoparticle matrix interfacial adhesion. It was found that the essential work of fracture (EWF) approach, usually characterizing fracture toughness of ductile materials, was no longer applicable to the nanocomposite samples because of the extreme crack blunting and tearing processes observed in the EWF tests. As an alternative approach, the specific essential work-related yield was used for assessment of the plane-strain toughness, as suggested in the literature. The results indicated that the addition of 1 vol.% nano-TiO₂ did not toughen the PP matrix at all. In this letter, we studied the fracture behavior of injection- molded PP composites filled with surface-modified nano-TiO₂ particles at different tensile rates. It was observed that a small amount of surface-modified nano-TiO₂ particles significantly affected the skin/core structure of injection-molded PP samples, and in turn, improved the whole fracture energy of the nanocomposites dramatically. Under tensile load, the notched injection-molded PP samples became too ductile to be characterized by the EWF approach validly.

Ibrahim et al. [10] studied that the effect of mineral surface nature on the mechanical properties of mineral-filled PP composites. This issue is still occupying a big part of the researchers thinking to find a proper solution, however, its difficulty returns to different factors playing roles in it. Among these factors are the filler surface, i.e., hydrophobicity

and hydrophilicity, functional groups on the surface, as well as mineral filler particle size distribution, and particle shape. Therefore, in the current study, the difference in mechanical properties for two mineral fillers; namely, silica and talc, differs in their surface and rheology properties were investigated. Results showed that the difference in the mechanical properties of the same matrix when the inorganic filler is different either in type or loading. In the present study, two minerals were used as fillers for PP matrix, namely; talc and silica. Different behavior of these two fillers in terms of their influence on the overall mechanical behavior of the mineral/PP composite was studied and correlated to the difference in the surface characteristics of both mineral fillers. Talc showed the better results in terms of Young's modulus and impact strength, where silica showed higher yield strength. On other hand, both fillers resulted in lowering the strain measures. The difference in behavior between talc/PP and silica/PP can be referred to unique properties of each mineral. In general, the introduction of inorganic fillers to PP leads not only to increase in toughness and ductility but also to an increase in stiffness and strength of the mineralfilled PP end-products which can greatly enlarge their engineering applications.

Jianfeng et al. [11] examined that the assistant effect of nano-CaCO₃ particles on the dispersion of TiO₂ pigment in PP composites. In this paper, nano-CaCO₃ synthesized by a high gravity reactive precipitation method was employed as a new pigment dispersant, blending with TiO₂ and other additives to prepare complex master batches for use in the coloring of PP. The influence of the synergism of CaCO₃ and TiO₂ on the performance of colored PP products is discussed. In conclusion, nano-CaCO₃ is an excellent pigment dispersant, which can partially replace TiO₂ pigments for PP resin coloring. Nano-CaCO₃ can prompt the dispersion of TiO₂ in polymer matrix, boosting the whiteness of the materials without a negative effect on the UV absorbency of the materials.

Zohrab et al. [12] examine the synthesis and morphological study of nanoparticles Ag/TiO₂ ceramic and bactericidal investigation of PP-Ag/TiO₂ composite. Structure of synthesized ceramic was characterized using different methods of spectroscopies including; X-ray diffraction (XRD), TEM, and scanning probe microscopy. The results

show that very fine silver particles were loaded on the titania dispersedly and also no crystalline change happened in the TiO_2 structure.

Jun et al. [13] studied the photocatalytic degradation of organic dyes by $\text{Er}^{3+}:\text{YAlO}_3/\text{TiO}_2$ composite under solar light. In this work, $\text{Er}^{3+}:\text{YAlO}_3/\text{TiO}_2$ composite was synthesized by a ultrasonic dispersion and liquid boil method. The $\text{Er}^{3+}:\text{YAlO}_3/\text{TiO}_2$ composite and pure TiO_2 powder were characterized by XRD. The degradation of different organic dyes was used to evaluate the photocatalytic activity of the $\text{Er}^{3+}:\text{YAlO}_3/\text{TiO}_2$ composite. It is found that the photocatalytic activity of $\text{Er}^{3+}:\text{YAlO}_3/\text{TiO}_2$ composite is much higher than that for the similar system with only TiO_2 . Moreover, this $\text{Er}^{3+}:\text{YAlO}_3/\text{TiO}_2$ composite provides a new way to take advantage of TiO_2 in sewage treatment aspects using solar light. Much attention has been paid to the photocatalytic degradation of dyes with TiO_2 particles due to its relatively low price, its chemical stability and nontoxicity. The $\text{Er}^{3+}:\text{YAlO}_3/\text{TiO}_2$ composite heat-treated at 500 °C for 60 min with 6.0 wt% $\text{Er}^{3+}:\text{YAlO}_3$ content exhibited a notably high photocatalytic activity in the degradation of organic dyes under solar light irradiation. The influences of $\text{Er}^{3+}:\text{YAlO}_3$ content, heat-treated temperature, heat-treated time and irradiation time on photodegradation process were investigated in detail.

Juhong et al. [14] examined the synthesis and characterization of bamboo-like CdS/TiO_2 nanotubes composites with enhanced visible-light photocatalytic activity. This CdS/TiO_2 nanotubes composite exhibited much higher visiblelight photocatalytic activity for the degradation of methylene blue than pure TiO_2 nanotubes and CdS nanoparticles, and the highest photodegradation efficiency after 6 h irradiation can reach 84.5%. It is inferred that the unique structure of CdS/TiO_2 nanotubes composites acts an important role for the improvement of their photocatalytic activity. As the most promising photocatalyst, TiO_2 materials are widely applied for the effective decomposition of organic pollutants in air and water, and also expected to play an important role in helping ease the energy crisis through effective utilization of solar energy based on photovoltaic and water-splitting devices. The characterized results indicated that CdS nanoparticles were formed in TiO_2 nanotubes, leading to a novel bamboo-like CdS/TNTs composite. It is deduced that the

space confinement of TNTs with 3.7 nm in diameter acts an important role in the formation of this kind of CdS/TNTs composite. Since the presence of CdS nanoparticles can extend the absorption edge to visible region at about 540 nm, together with the high specific area of TiO₂ nanotubes, the resultant CdS/TNTs composites exhibited high efficiency for the degradation of methylene blue under visible illumination.

Preparation and characterizations of TiO₂/organically modified silane composite materials produced by the Sol-Gel method were reported by Wenxiu et al. [15]. In this report high optical quality waveguiding films on different substrates, including silicon, gallium arsenide, silica/silicon substrates, and microscope glass slides, were prepared from high titanium content (0.2 molar) γ -glycidoxypropyltrimethoxysilane at low temperature. SEM, atomic force microscopy (AFM), differential thermal analysis (DTA), thermal gravimetric analysis (TGA), Fourier transform infrared spectroscopy (FTIR) and X-ray photoelectron spectroscopy (XPS) have been used to investigate the optical and structural properties of the composite films. The TGA/DTA results showed that the organic compounds in the film would tend to decompose in the temperature range from 200±C to 500±C. SEM.

Ghulam et al. [16] investigated the photocatalytic disinfection of water with Ag–TiO₂ nanocrystalline composite. It is seen that the relatively small loading of Ag has not caused any UV–vis spectral shift but has enhanced the rate of photocatalytic antibacterial action of TiO₂, presumably by electron trapping.

Nanostructured carbon nanotube/TiO₂ composite coatings using electrophoretic deposition (EPD) were studied by Johann et al. [17]. In this report EPD has been used to combine multi-walled carbon nanotubes of diameter in the range 20–30 nm and commercially available TiO₂ nanoparticles (23 nm particle size) in composite films. Laminate coatings with up to four layers were produced by sequential EPD, while composite coatings were obtained by electrophoretic co-deposition of carbon nanotubes and TiO₂ nanoparticles, respectively. SEM was used to characterize the resultant microstructures. The mechanism of EPD of carbon nanotube/TiO₂ nanoparticle composites is discussed.

Moroz et al. [18] studied that synthesis and microstructure evolution of nano-titania doped silicon coatings. Titania is a widely known and readily available photocatalyst. Titania's ability to absorb light energy makes it a viable material to implant in a matrix of crystalline Silicon in order to increase the efficiency of photovoltaic cells. Recent focus in sources of alternative energy, such as solar power by using photovoltaic solar cells, has generated renewed interest in the photocatalytic applications of TiO₂. The increase in efficiency of the photovoltaic cell due to the embedded titania particles is proportional to the surface area of the Titania. Therefore, nanoparticles of titania are expected to yield a large surface area due to their small size, and still maintain the physical integrity of the silicon.

Synthesis of silica supported titania nanocomposite in controllable phase content and morphology are studied by Lim Yew Von et al [19]. The effects of growth conditions, such as the annealing temperature and silicon concentration on the particle size and phase content, were systematically studied by using AFM, Raman spectroscopy, XRD and XPS. The results indicate that the silicon concentration is a dominant factor in the morphology, crystallization and phase transformation of these nanocomposites.

Amorphous MnO₂-TiO₂ composites as sorbents for Sr²⁺ and UO₂ are studied by Oksana et al [20]. Significant progress has been achieved in this field during the last decade, and several novel materials with high values of distribution coefficients. The principles of template synthesis prove their usefulness in the synthesis of hydrous, amorphous MnO₂-TiO₂ materials. Binary composites have much greater affinity to Sr²⁺ ions at pH=7 than single oxides, probably, due to formation of an amorphous "solid solution" of MnO₂ and TiO₂.

Tadashi et al. [21] showed the Polyethylene terephthalate (PET) fiber fabrics modified with bioactive titanium oxide for bone substitutes. A rectangular specimen of PET was soaked in a titania solution composed of titanium isopropoxide, water, ethanol and nitric acid at 25 °C for 1 h. An amorphous titanium oxide was formed uniformly on the surface

of PET specimen, but did not form an apatite on its surface in a simulated body fluid (SBF) within 3 d. The PET plate formed with the amorphous titanium oxide was subsequently soaked in water or HCl solutions with different concentrations at 80 °C for different periods of time. The titanium oxide on PET was transformed into nano-sized anatase by the water treatment and into nano-sized brookite by 0.10 M HCl treatment at 80 °C for 8 d.

Recently, metals such as titanium metal and its alloys [22] and tantalum metal [23] have been found to bond to living bone after being exposed to a NaOH solution and heat treatments. These materials are called bioactive materials, and being used clinically as important bone substitutes. However, they have much higher elastic moduli than human bone and cannot be easily deformed. In such case, the surrounding bone is liable to be resorbed, since the stress is mainly borne by these materials, but not by the surrounding bones. Therefore, the contemporary desire is to develop bioactive materials with low elastic moduli.

Hou Hongmei et al [24] observed the Supercritically treated TiO₂-activated carbon composites for cleaning ammonia. Supercritically treated TiO₂-activated carbon (Sc-TiO₂-AC) composites were studied for their adsorption and photocatalytic activities toward gaseous ammonia (NH₃). The experiments were carried out at 26°C using a black lamp. The Sc-TiO₂-AC composites attained higher photocatalytic activities than supercritically treated TiO₂ (Sc-TiO₂). NH₃ was found out to be converted by the Sc-TiO₂-AC composites to compounds such as N₂, N₂O, NO₂, and NO₃. This study found that Sc-TiO₂-AC composites have very high photocatalytic activity for the decomposition of NH₃. In the decomposition process, NH₃ is successfully converted to harmless and odorless compounds.

He et al. [25] studied the Structure and photochromic properties of molybdenum phosphoric acid/TiO₂ composite films. The structure and constitute of composite thin films were studied with FTIR, AFM and XRD patterns, respectively. The photochromic behavior and mechanism of composite thin films were investigated with ultraviolet-visible spectra (UV-vis) and electron spin resonance (ESR).

Nazeri et al. [26] studied the synthesis and properties of cerium and TiO₂. The effect of processing parameters such as the atmosphere of heat-treatment, and temperature on the microstructure and crystal structure of the films and powders of ceria and titania was investigated. XRD was used to identify the crystal structure of films and powders upon heat-treatment. Electrochemical measurements in sodium chloride (NaCl), and analytical techniques such as SEM and EDX were used to evaluate the corrosion performance and pitting morphology of coated samples. A composite coating of ceria and titania was able to prevent crevice corrosion and increase the pitting resistance of the 304 stainless steel relative to the uncoated substrate. It was possible to obtain good quality multilayer titania films with an underlayer of ceria. The ceria undercoat seemed to greatly enhance the resistance of the substrate to oxidation. The role of ceria and the mechanism by which it works was not studied in this work. Further examination of the microstructure, surface and interface is required to better understand the mechanisms and reasons for such behavior. However, in light of all previous works reported on the inhibition effects of ceria on high temperature oxidation of stainless steels, this behavior was expected.

1.3 Objectives

This work is aimed at preparing iPP-TiO₂ composites using low cost iPP and TiO₂ by extrusion molding and extrusion cum compression molding method. In order to study the possibility of superior performance and reduced costs, iPP and TiO₂ are used and different sets of composites are prepared by mixing 10, 20, 30, 40 and 50 wt% TiO₂ with iPP by extrusion molding technique. The mechanical properties, such as stress-strain behavior, tensile strength, elongation-at-break (%) of the iPP-TiO₂ are studied. The micromechanical property, *H*, of the composites is also be investigated. AC dielectric properties of different composites samples are investigated. The thermal analysis is performed to observe the thermal degradation in the different composites. The mechanical, micromechanical and AC electrical properties of the composites are correlated in relation to the TiO₂ content in the composites to understand the fundamental processes involved in modifying the above properties. This understanding of the

mechanical and electrical behaviors of the composites is useful to find out suitability of these materials for household and technological applications.

1.4 Thesis lay-out

The thesis consists of five chapters. Chapter one gives a general introduction about the iPP-TiO₂ composites. This chapter also presents a brief review of the earlier works done on iPP-TiO₂ composites with aims and objectives of the thesis. Chapter two describes the general aspects of polymer, composites, polypropylene and titanium dioxide. The experimental details of the different characterization techniques are described in chapter three. Chapter four presents the experimental results of the different measurement processes. Chapter five is the concluding chapter giving the summary of the experimental results with suggestions for the future work to be done.

CHAPTER 2 FUNDAMENTAL ASPECT OF POLYMER, POLYPROPYLENE, TiO₂ AND COMPOSITES

2.1 Polymers	
2.1.1 Definition of Polymer	12
2.1.2 Classification of Polymers	12
2.2 Polypropylene	14
2.2.1 Chemical and Physical Properties of Polypropylene	15
2.2.2 Electrical Properties	17
2.2.3 Mechanical Properties	17
2.2.4 Thermodynamic Properties	18
2.2.5 Application of Polypropylene	19
2.3 Titanium dioxide	21
2.3.1 Physical and Chemical Characteristics	22
2.3.2 Applications of TiO₂	23
2.4 Composites	
2.4.1 Definition	25
2.4.2 Different types of Composite Materials	26
2.5 Theory of Mechanical Properties of Composites	
2.5.1 Concepts of Stress and Strain	28
2.5.2 Stress-strain Behavior	30
2.5.3 Anelasticity	32
2.5.4 Tensile Properties	33
2.5.5 True Stress and Strain	33
2.5.6 Elongation	33
2.5.7 Hardness	34
2.6 Thermal Analysis	
2.6.1 Theory of thermal analysis	34
2.6.2 Differential Thermal analysis (DTA)	34
2.6.3 Thermogravimetric analysis (TGA)	37
2.6.4 Differential Scanning Calorimetry (DSC)	38
2.6.5 Scanning Electron Microscopy (SEM)	39
2.7 Dielectrics	40
2.7.1 Dielectric Constant	41
2.7.2 Dielectric loss	41
2.7.3 Debye relaxation	42

CHAPTER 2

2.1 Polymers

2.1.1 Definition of Polymer

A polymer is a large molecule (macromolecule) composed of repeating structural units, called monomers, typically connected by covalent chemical bonds. Whereas the term polymer is sometimes taken to refer to plastics, it actually encompasses a large class of natural and synthetic materials with a wide variety of properties.

Due to the extraordinary range of properties of polymeric materials, polymers play an essential and ubiquitous role in everyday life. This role ranges from familiar synthetic plastics and elastomers to natural biopolymers such as nucleic acids and proteins that are essential for life.

Natural polymeric materials such as shellac, amber, and natural rubber have been used for centuries. A variety of other natural polymers exist, such as cellulose, which is the main constituent of wood and paper. The list of synthetic polymers includes synthetic rubber, bakelite, neoprene, nylon, PVC, polystyrene, polyethylene, PP, polyacrylonitrile, PVB, silicone, and many more.

Most commonly, the continuously linked backbone of a polymer used for the preparation of plastics consists mainly of carbon atoms. A simple example is polyethylene, whose repeating unit is based on ethylene monomer. However, other structures do exist; for example, elements such as silicon form familiar materials such as silicones, examples being Silly Putty and waterproof plumbing sealant. Oxygen is also commonly present in polymer backbones, such as those of polyethylene glycol, polysaccharides (in glycosidic bonds), and DNA

2.1.2 Classification of Polymers

There are two types of polymers: synthetic and natural. Synthetic polymers are derived from petroleum oil, and made by scientists and engineers. Examples of synthetic polymers include nylon, polyethylene, polyester, Teflon, and epoxy.

Natural polymers occur in nature and can be extracted. They are often water-based.

Examples of naturally occurring polymers are silk, wool, DNA, cellulose and proteins.

Natural polymers include:

Proteins - silk, collagen, keratin.

Carbohydrates - cellulose, starch, glycogen

DNA – RNA

synthetic polymers includes

Classification of Polymers:

Homopolymers - consist of chains with identical bonding linkages to each monomer unit. This usually implies that the polymer is made from all identical monomer molecules.

These may be represented as: - [A-A-A-A-A-A]-

Copolymers - consist of chains with two or more linkages usually implying two or more different types of monomer units.

These may be represented as: -[A-B-A-B-A-B]-

Polymers are further classified by the reaction mode of polymerization, these include:

Addition Polymers - the monomer molecules bond to each other without the loss of any other atoms. Alkene monomers are the biggest groups of polymers in this class.

Condensation Polymers - usually two different monomer combine with the loss of a small molecule, usually water. Polyesters and polyamides (nylon) are in this class of polymers. Polyurethane Foam in graphic.

Classification based upon the physical property related to heating:

Thermoplastics - plastics that soften when heated and become firm again when cooled.

This is the more popular type of plastic because the heating and cooling may be repeated.

Thermosets - plastics that soften when heated and can be molded, but harden permanently. They will decompose when reheated. An example is Bakelite, which is used in toasters, handles for pots and pans, dishes, electrical outlets and billiard balls

2.2 Polypropylene

PP is an economical thermoplastic polymer that offers a combination of outstanding physical, chemical, mechanical, thermal and electrical properties not found in any other thermoplastic. Compared to low or high density polyethylene, it has a lower impact strength, but superior working temperature and tensile strength.

PP possesses excellent resistance to organic solvents, degreasing agents and electrolytic attack. It has lower impact strength, but its working temperatures and tensile strength are superior to low or high density polyethylene. It is light in weight, resistant to staining, and has a low moisture absorption rate. This is a tough, heat-resistant, semi-rigid material, ideal for the transfer of hot liquids or gases. It is recommended for vacuum systems and where higher heats and pressures are encountered. It has excellent resistance to acids and alkalies, but poor aromatic, aliphatic and chlorinated solvent resistance.

PP made by the chemical industry and used in a wide variety of applications, including packaging, textiles (e.g. ropes, thermal underwear and carpets), stationery, plastic parts and reusable containers of various types, laboratory equipment, loudspeakers, automotive components, and polymer banknotes. Figure 2.1 shows the chemical structure of PP. An addition polymer made from the monomer propylene, it is rugged and unusually resistant to many chemical solvents, bases and acids. In 2007, the global market for PP had a volume of 45.1 million tons, which led to a turnover of about 65 billion US-dollars (47.4 billion Euro).

Physical Properties of PP:

Molecular formula: (C₃H₆)_n

Density: 0.855 g/cm³, amorphous
0.946 g/cm³, crystalline

Melting point: 130–171 °C

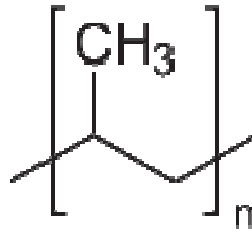


Figure 2.1: The chemical structure of PP.

Isotactic polypropylene (iPP) is a highly crystallizable, low cost and balance-strength polymer. The crystallization behavior and structural development in iPP has received considerable attention because it has potential applications in the area of composite fabrications and in some cases as replacement of low-end-use engineering polymers [1-3].

2.2.1 Chemical and Physical Properties of Polypropylene

Chemical and physical properties

Most commercial PP is isotactic and has an intermediate level of crystallinity between that of low-density polyethylene (LDPE) and high-density polyethylene (HDPE). PP is normally tough and flexible, especially when copolymerized with ethylene. This allows PP to be used as an engineering plastic, competing with materials such as ABS. PP is reasonably economical, and can be made translucent when uncolored but is not as readily made transparent as polystyrene, acrylic, or certain other plastics. It is often opaque or colored using pigments. PP has good resistance to fatigue.

The melting of PP occurs as a range, so a melting point is determined by finding the highest temperature of a differential scanning calorimetry (DSC) chart. Perfectly isotactic PP has a melting point of 171 °C. Commercial isotactic PP has a melting point that ranges from 160 to 166 °C, depending on atactic material and crystallinity. Syndiotactic PP with a crystallinity of 30% has a melting point of 130 °C (266 °F).

There are three general types of PP:

- i) homopolymer,
- ii) random copolymer, and
- iii) block copolymer.

Degradation

PP is liable to chain degradation from exposure to heat and UV radiation such as that present in sunlight. Oxidation usually occurs at the tertiary carbon atom present in every repeat unit. A free radical is formed here, and then reacts further with oxygen, followed by chain scission to yield aldehydes and carboxylic acids. In external applications, it shows up as a network of fine cracks and crazes that become deeper and more severe with time of exposure.

For external applications, UV-absorbing additives must be used. Carbon black also provides some protection from UV attack. The polymer can also be oxidized at high temperatures, a common problem during molding operations. Anti-oxidants are normally added to prevent polymer degradation.

Manufacturing

Melt processing of PP can be achieved via extrusion and molding. Common extrusion methods include production of melt-blown and spun-bond fibers to form long rolls for future conversion into a wide range of useful products, such as face masks, filters, nappies (diapers) and wipes.

The most common shaping technique is injection molding, which is used for parts such as cups, cutlery, vials, caps, containers, housewares, and automotive parts such as batteries. The related techniques of blow molding and injection-stretch blow molding are also used, which involve both extrusion and molding.

The large number of end-use applications for polypropylene are often possible because of the ability to tailor grades with specific molecular properties and additives during its manufacture. For example, antistatic additives can be added to help polypropylene surfaces resist dust and dirt.

2.2.2 Electrical Properties

Table 2.1: Electrical Properties

<i>ELECTRICAL</i>	
Dielectric strength (V/mil) short time, 1/8-in. thick	500-660
Dielectric constant at 1kHz	2.2-2.6
Dissipation factor at 1kHz	0.0005-0.0018
Volume resistivity (ohm-cm) at 73°F, 50% RH	10~17
Arc resistance(s)	160

2.2.3 Mechanical Properties

The bulk properties of a polymer are those most often of end-use interest. These are the properties that dictate how the polymer actually behaves on a macroscopic scale. The different characteristics of the mechanical properties are described below:

Table 2.2: Mechanical properties

MECHANICAL PROPERTIES	
Tensile strength (psi)	5,000
Elongation (%)	10-20
Tensile modulus (10~5 psi)	1.6
Flexural modulus (10~5 psi)	1.7-2.5
Impact strength, izod (ft-lb/in. of notch)	0.5-2.2
Hardness, Rockwell R	80-110

Tensile strength

The tensile strength of a material quantifies how much stress the material will endure before suffering permanent deformation. This is very important in applications that rely upon a polymer's physical strength or durability. For example, a rubber band with a higher tensile strength will hold a greater weight before snapping. In general, tensile strength increases with polymer chain length and crosslinking of polymer chains.

Young's modulus of elasticity

Young's Modulus quantifies the elasticity of the polymer. It is defined, for small strains, as the ratio of rate of change of stress to strain. Like tensile strength, this is highly relevant in polymer applications involving the physical properties of polymers, such as rubber bands. The modulus is strongly dependent on temperature.

Microstructure

The microstructure of a polymer (sometimes called configuration) relates to the physical arrangement of monomer residues along the backbone of the chain. These are the elements of polymer structure that require the breaking of a covalent bond in order to change. Structure has a strong influence on the other properties of a polymer. For example, two samples of natural rubber may exhibit different durability, even though their molecules comprise the same monomers.

2.2.4 Thermodynamic Properties

Melting point

The term *melting point*, when applied to polymers, suggests not a solid-liquid phase transition but a transition from a crystalline or semi-crystalline phase to a solid amorphous phase. Though abbreviated as simply T_m , the property in question is more properly called the crystalline melting temperature. Among synthetic polymers, crystalline melting is only discussed with regards to thermoplastics, as thermosetting polymers will decompose at high temperatures rather than melt.

Glass transition temperature

A parameter of particular interest in synthetic polymer manufacturing is the glass transition temperature (T_g), which describes the temperature at which amorphous polymers undergo a transition from a rubbery, viscous amorphous liquid, to a brittle, glassy amorphous solid. The T_g may be engineered by altering the degree of branching or crosslinking in the polymer or by the addition of plasticizer.

2.2.5 Application of Polypropylene

Since PP is resistant to fatigue, most plastic living hinges, such as those on flip-top bottles, are made from this material. However, it is important to ensure that chain molecules are oriented across the hinge to maximize strength. Very thin sheets of PP are used as a dielectric within certain high-performance pulse and low-loss RF capacitors.

PP is used in the manufacturing piping systems; both ones concerned with high-purity and ones designed for strength and rigidity. This material is often chosen for its resistance to corrosion and chemical leaching, its resilience against most forms of physical damage, including impact and freezing, its environmental benefits, and its ability to be joined by heat fusion rather than gluing.

Many plastic items for medical or laboratory use can be made from PP because it can withstand the heat in an autoclave. Its heat resistance also enables it to be used as the manufacturing material of consumer-grade kettles. Food containers made from it will not melt in the dishwasher, and do not melt during industrial hot filling processes.

PP can also be made into disposable bottles to contain liquid, powdered, or similar consumer products, although HDPE and PET are commonly also used to make bottles. Plastic pails, car batteries, wastebaskets, pharmacy prescription bottles, cooler containers, dishes and pitchers are often made of polypropylene or HDPE, both of which commonly have rather similar appearance, feel, and properties at ambient temperature. A common application for PP is as biaxially oriented polypropylene (BOPP). These BOPP sheets are used to make a wide variety of materials including clear bags. When PP is biaxially oriented, it becomes crystal clear and serves as an excellent packaging material for artistic and retail products. PP, highly colorfast, is widely used in manufacturing carpets, rugs and mats to be used at home. PP is widely used in ropes, distinctive because they are light enough to float in water. For equal mass and construction, polypropylene rope is similar in strength to polyester rope. Polypropylene costs less than most other synthetic fibers.

PP is also used as an alternative to polyvinyl chloride (PVC) as insulation for electrical cables for LSZH cable in low-ventilation environments, primarily tunnels. This is because it emits less smoke and no toxic halogens, which may lead to production of acid in high-temperature conditions. PP is also used in particular roofing membranes as the waterproofing top layer of single-ply systems as opposed to modified-bit systems. PP is most commonly used for plastic moldings, wherein it is injected into a mold while molten, forming complex shapes at relatively low cost and high volume; examples include bottle tops, bottles, and fittings.

It can also be produced in sheet form, which is been widely used for the production of stationery folders, packaging, and storage boxes. The wide color range, durability, cost, and resistance to dirt make it ideal as a protective cover for papers and other materials. It is used in Rubik's cube stickers because of these characteristics.

The availability of sheet PP has provided an opportunity for the use of the material by designers. The light-weight, durable, and colorful plastic makes an ideal medium for the creation of light shades, and a number of designs have been developed using interlocking sections to create elaborate designs.

PP sheets are a popular choice for trading card collectors; these come with pockets (nine for standard-size cards) for the cards to be inserted and are used to protect their condition and are meant to be stored in a binder. Expanded polypropylene (EPP) is a foam form of polypropylene. EPP has very good impact characteristics due to its low stiffness; this allows EPP to resume its shape after impacts. EPP is extensively used in model aircraft and other radio controlled vehicles by hobbyists. PP is used in the manufacture of loudspeaker drive units. Its use was pioneered by engineers at the BBC and the patent rights subsequently purchased by Mission Electronics for use in their Mission Freedom Loudspeaker and Mission 737 Renaissance loudspeaker. PP fibres are used as a concrete additive to increase strength and reduce cracking and spalling.

Clothing

PP is a major polymer used in nonwovens, with over 50% used for diapers or sanitary products where it is treated to absorb water (hydrophilic) rather than naturally repelling water (hydrophobic). Other interesting non-woven uses include filters for air, gas, and liquids in which the fibers can be formed into sheets or webs that can be pleated to form cartridges or layers that filter in various efficiencies in the 0.5 to 30 micrometre range.

In New Zealand, in the US military, and elsewhere, polypropylene, or 'polypro', has been used for the fabrication of cold-weather base layers, such as long-sleeve shirts or long underwear. PP is also used in warm-weather gear such as some. The material has recently been introduced into the fashion industry through the work of designers such as Anoush Waddington, who have developed specialized techniques to create jewelry and wearable items from polypropylene.

Medical

Its most common medical use is in the synthetic, nonabsorbable suture Prolene, manufactured by Ethicon Inc. PP has been used in hernia and pelvic organ prolapse repair operations to protect the body from new hernias in the same location. A small patch of the material is placed over the spot of the hernia, below the skin, and is painless and is rarely, if ever, rejected by the body.

2.3 Titanium dioxide (TiO₂)

Titanium dioxide (TiO₂) pigment is a fine white powder. When used in paints, plastics or paper, it provides for maximum whiteness and opacity. It gives paint high hiding power, meaning the ability to mask or hide a substrate. It does this more effectively than any other white pigment. Today, TiO₂ pigment is by far the most important material used by the paints and plastics industry for whiteness and opacity. These unique properties are derived from the refractive index of TiO₂. The refractive index expresses the ability to bend and scatter light. TiO₂ has the highest refractive index of any material known to man, greater even than diamond. To take advantage of this property, TiO₂ must be mined,

refined and ground to a fine, uniform particle size. Titanium dioxide, also known as titanium(IV) oxide or titania, is the naturally occurring oxide of titanium, chemical formula TiO₂. It has a wide range of applications, from paint to sunscreen to food colouring.

Production

Crude TiO₂ is purified via converting to titanium tetrachloride in the chloride process. In this process, the crude ore (containing at least 70% TiO₂) is reduced with carbon, oxidized with chlorine to give titanium tetrachloride; i.e., carbothermal chlorination. This titanium tetrachloride is distilled, and re-oxidized in a pure oxygen flame or plasma at 1500–2000 K to give pure titanium dioxide while also regenerating chlorine. Aluminium chloride is often added to the process as a rutile promotor; the product is mostly anatase in its absence.

2.3.1 Physical and Chemical Characteristics

TiO₂ is usually associated with iron, mostly as ilmenite. It is also mined in one of the pure forms, rutile beach sand. The map below shows the world's most important deposits of the basic raw materials used in the manufacture of TiO₂ pigments.

Molecular formula: TiO₂

Molar mass: 79.866 g/mol

White solid: Appearance

Density: 4.23 g/cm³

Melting point: 1843 °C

Boiling point: 2972 °C

2.3.2 Applications of TiO₂

Pigment

TiO₂ is the most widely used white pigment because of its brightness and very high refractive index ($n = 2.7$), in which it is surpassed only by a few other materials. Approximately 4 million tons of pigmentary TiO₂ are consumed annually worldwide. When deposited as a thin film, its refractive index and colour make it an excellent reflective optical coating for dielectric mirrors. TiO₂ is also an effective opacifier in powder form, where it is employed as a pigment to provide whiteness and opacity to products such as paints, coatings, plastics, papers, inks, foods, medicines (i.e. pills and tablets) as well as most toothpastes. In paint, it is often referred to offhandedly as "the perfect white", "the whitest white", or other similar terms. Opacity is improved by optimal sizing of the TiO₂ particles.

TiO₂ is often used to whiten skimmed milk; this has been shown statistically to increase skimmed milk's palatability. In cosmetic and skin care products, titanium dioxide is used as a pigment, sunscreen and a thickener. It is also used as a tattoo pigment and in styptic pencils. This pigment is used extensively in plastics and other applications for its UV resistant properties where it acts as a UV absorber, efficiently transforming destructive UV light energy into heat. In ceramic glazes TiO₂ acts as an opacifier and seeds crystal formation. TiO₂ is found in almost every sunscreen with a physical blocker because of its high refractive index, its strong UV light absorbing capabilities and its resistance to discolouration under ultraviolet light. This advantage enhances its stability and ability to protect the skin from ultraviolet light.

Photocatalyst

Recently it has been found that TiO₂, when spiked with nitrogen ions or doped with metal oxide like tungsten trioxide, is also a photocatalyst under either visible or UV light. The strong oxidative potential of the positive holes oxidizes water to create hydroxyl radicals. It can also oxidize oxygen or organic materials directly. TiO₂ is thus added to paints, cements, windows, tiles, or other products for its sterilizing, deodorizing and anti-fouling

properties and is used as a hydrolysis catalyst. It is also used in dye-sensitized solar cells, which are a type of chemical solar cell (also known as a Graetzel cell).

TiO₂ has potential for use in energy production: as a photocatalyst, it can

- carry out hydrolysis; i.e., break water into hydrogen and oxygen. Were the hydrogen collected, it could be used as a fuel.
- TiO₂ can also produce electricity when in nanoparticle form. Research suggests that by using these nanoparticles to form the pixels of a screen, they generate electricity when transparent and under the influence of light. If subjected to electricity on the other hand, the nanoparticles blacken, forming the basic characteristics of a LCD screen.
- In 1995 Fujishima and his group discovered the superhydrophilicity phenomenon for titanium dioxide coated glass exposed to sun light.^[19] This resulted in the development of self-cleaning glass and anti-fogging coatings.

TiO₂ offers great potential as an industrial technology for detoxification or remediation of wastewater due to several factors.

1. The process occurs under ambient conditions very slowly; direct UV light exposure increases the rate of reaction.
2. The formation of photocyclized intermediate products, unlike direct photolysis techniques, is avoided.
3. Oxidation of the substrates to CO₂ is complete.
4. The photocatalyst is inexpensive and has a high turnover.

Electronic data storage medium

Researchers at the University of Tokyo, Japan have created a 25 terabyte titanium oxide-based disc.

2.4 Composites

2.4.1 Definition

A composite material is a material made up of two or more materials that are combined in a way that allows the materials to stay distinct and identifiable. The purpose of composites is to allow the new material to have strengths from both materials, often times covering the original materials' weaknesses. Composites are different from alloys because alloys are combined in such a way that it is impossible to tell one particle, element, or substance from the other. Some common composite materials include concrete, fiberglass, mud bricks, and natural composites such as rock and wood.

In its most basic form a composite material is one, which is composed of at least two elements working together to produce material properties that are different to the properties of those elements on their own. In practice, most composites consist of a bulk material (the 'matrix'), and a reinforcement of some kind, added primarily to increase the strength and stiffness of the matrix. This reinforcement is usually in fibre form.

A composite is any material made of more than one component. There are a lot of composites around us. Composites materials, usually man-made, that are a three-dimensional combination of at least two chemically distinct materials, with a distinct interface separating the components, created to obtain properties that cannot be achieved by any of the components acting alone.

Fibers and Matrix

Composites are combinations of two materials in which one of the materials, called the reinforcing phase, is in the form of fibers, sheets, or particles, and are embedded in the other materials called the matrix phase.

The reinforcing material and the matrix material can be metal, ceramic, or polymer. Typically, reinforcing materials are strong with low densities while the matrix is usually a ductile, or tough, material. If the composite is designed and fabricated correctly, it combines the strength of the reinforcement with the toughness of the matrix to achieve a

combination of desirable properties not available in any single conventional material. Examples of some current application of composites include the diesel piston, brake-shoes and pads, tires, etc. Most composites have strong, stiff fibres in a matrix which is weaker and less stiff. The objective is usually to make a component which is strong and stiff, often with a low density. Commercial material commonly has glass or carbon fibres in matrices based on thermosetting polymers, such as epoxy or polyester resins. Sometimes, thermoplastic polymers may be preferred, since they are mouldable after initial production. There are further classes of composite in which the matrix is a metal or a ceramic. For the most part, these are still in a developmental stage, with problems of high manufacturing costs yet to be overcome. Furthermore, in these composites the reasons for adding the fibres (or, in some cases, particles) are often rather complex; for example, improvements may be sought in creep, wear, fracture toughness, thermal stability, etc. The sand on a beach is an example of a natural composite material.

2.4.2 Different types of Composite Materials

Types

Composite materials are usually classified by the type of reinforcement they use. This reinforcement is embedded into a matrix that holds it together. The reinforcement is used to strengthen the composite. For example, in a mud brick, the matrix is the mud and the reinforcement is the straw.

Mud Bricks

One type of very old composite material invented by early humans was the mud brick. A normal mud brick is sturdy and resistant to compression, but can break if bent. Straw is a material that has excellent tensile strength, meaning that it resists stretching. By combining both, early humans were able to create composite mud bricks that could resist weight and compression as well as stretching.

Concrete

Concrete is a composite material made of cement, sand, stones and water. Combined, concrete is stronger than any one of these materials. Concrete is used heavily in building and road construction.

Fiberglass

Fiberglass is a material made of tiny glass shards held together by resin and other components. In the automotive industry, fiberglass is important for making body kits. The body shell for a car is made up of different layers of fiberglass, such as a gel-coat layer, tissue layer, matting and cloth. The final product is a complete, waterproof, lightweight and strong body kit. Fiberglass can also be a less expensive alternative to other materials.

Natural Composites

Composites can be easily found in nature. Wood is an example of a composite because cellulose fibers are held together by substance called lignin. These fibers can be found in cotton and thread, but it's the bonding power of lignin in wood that makes it much tougher. Another natural composite is rock and sand, materials used in concrete. Rock is just smaller rocks held together, and sand is made of small grains.

Classification:

The most common man-made composites can be divided into three main groups:

- Polymer Matrix Composites (PMC's) – These are the most common and will be discussed here. Also known as FRP - Fibre Reinforced Polymers (or Plastics) – these materials use a polymer-based resin as the matrix, and a variety of fibres such as glass, carbon and aramid as the reinforcement.
- Metal Matrix Composites (MMC's) - Increasingly found in the automotive industry, these materials use a metal such as aluminium as the matrix, and reinforce it with fibres such as silicon carbide.

- Ceramic Matrix Composites (CMC's) - Used in very high temperature environments, these materials use a ceramic as the matrix and reinforce it with short fibres, or whiskers such as those made from silicon carbide and boron nitride.

2.5 Theory of Mechanical Properties of Composites

2.5.1 Concepts of Stress and Strain

Stress

In mechanics, **stress** is a measure of the internal forces acting within a deformable body. Quantitatively, it is a measure of the average force per unit area of a surface within the body on which internal forces act. These internal forces are produced between the particles in the body as a reaction to external forces applied on the body.

Beyond certain limits of material strength, this can lead to a permanent change of shape or physical failure.

Stress can occur in liquids, gases and solids. Liquids and gasses support normal stress (pressure), but flow under shear stress. Solids support both shear and normal stress, with brittle materials failing under normal stress and plastic or ductile materials failing under shear stress.

Engineering Stress:

A common application of the stress concept is termed the engineering stress. This particular expression, which is used in many design calculations and analyzes is given as follows:

$$a = P/A \quad (1)$$

The only modification to our basic stress equation is A, which represents the original area therefore, engineering stress treats cross sectional area as a constant, P is the tensile force. Although it is not completely accurate for elastic striations in the loading direction the corresponding changes in cross sectional area are generally small.

True Stress:

The concept of engineering stress treats the area under consideration as a constant (A_0). In reality however the area does not remain constant. And in the case of an axially loaded tensile bar, gradually decreases as the stress.

The true Stress therefore can be expressed as follows:

$$a_{tr} = P/A_t \quad (2)$$

where A_t is the actual instantaneous area over which the force is acting.

Ordinarily, a_{tr} is greater than a .

Strain:

Strain in physical sciences and engineering, number that describes relative deformation or change in shape and size of elastic, plastic, and fluid materials under applied forces. The deformation, expressed by strain, arises throughout the material as the particles (molecules, atoms, ions) of which the material is composed are slightly displaced from their normal position.

Strains may be divided into normal strains and shear strains on the basis of the forces that cause the deformation. A normal strain is caused by forces perpendicular to planes or cross-sectional areas of the material, such as in a volume that is under pressure.

Engineering Strain:

The response of atoms to deformation by mechanical forces is examined. In this concept of atomic displacement is extended to bulk engineering materials, we can define the deformation in terms of the original dimensions of the material under consideration in other words, in ratio of the dimensional change to the original dimension.

True Strain:

Instantaneous % of change in length of specimen in mechanical test. It is equal to the natural logarithm of the ratio of length at any instant to original length.

True-stress-true-strain curve

If the strain measurement is also based on instantaneous measurements, the curve, which is obtained, is known as a true-stress-true-strain curve. This is also known as a flow curve since it represents the basic plastic-flow characteristics of the material.

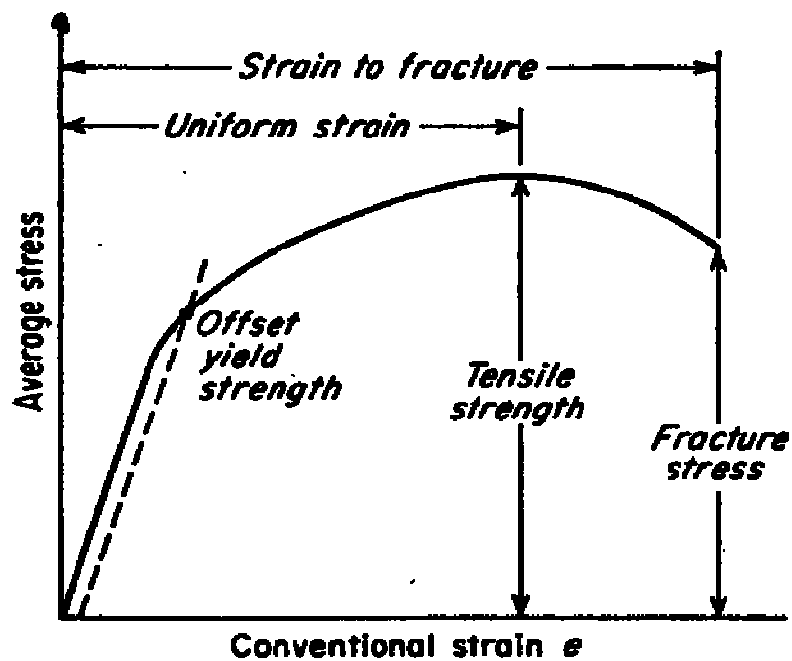


Figure 2.2: The true stress-true strain curve

2.5.2 Stress-strain Behavior

Deformation of Materials

When an engineering material (composite) is subjected to forces its atoms may be displaced from their equilibrium position. Any displacement from the position results in an energy increase. This requires work to create the displacement. It is clear that displacement premise holds whether the material is stretched causing the atoms to

separate. Thus bringing the attractive forces into play or compressed bringing the atoms closer together and causing repulsion.

Types of deformation

1. Elastic deformation

Description: The displacement of atoms from the equilibrium positions constitutes deformation. Such deformation is termed elastic if the atoms can resume their equilibrium positions when the imposed forces are released. For example: Rubber. A relatively small tensile force tends to pull the atoms apart producing elastic deformation. However when the force is released the atoms resume their equilibrium positions and no deformation remains. The material is restored to its initial conditions.

2. Plastic deformation

On the other hand if the engineering material undergoes deformation which exceeds the elastic, capability to restore the atoms to their equilibrium positions, the deformation is permanent and termed Plastic. Plastic deformation is non recoverable and leaves the atoms permanently displaced from their original positions where the forces are released.

Deformation of material may be entirely elastic or elastic plus plastic. Plastic deformation of engineering is permanent in the work or energy must be supplied to restore the atoms to their original equilibrium position. For instance the effect of these type of deformation can be found by thermal treatments. The deformation may then consist of the combined elastic and plastic portion. In this case, removal of the load producing the deformation results in recovery of the elastic portion, while the plastic portion remains.

Hooke's Law

Hooke's law accurately models the physical properties of common mechanical springs for small changes in length. Hooke's law describes how far the spring will stretch with a specific force.

In mechanics, and physics, **Hooke's law** of elasticity is an approximation that states that the extension of a spring is in direct proportion with the load applied to it. Many

materials obey this law as long as the load does not exceed the material's elastic limit. Materials for which Hooke's law is a useful approximation are known as linear-elastic materials. Hooke's law in simple terms says that strain is directly proportional to stress.

Mathematically, Hooke's law states that

$$F = -kx$$

where

x is the displacement of the end of the spring from its equilibrium position.

F is the restoring force exerted by the material

and k is a constant called the spring constant.

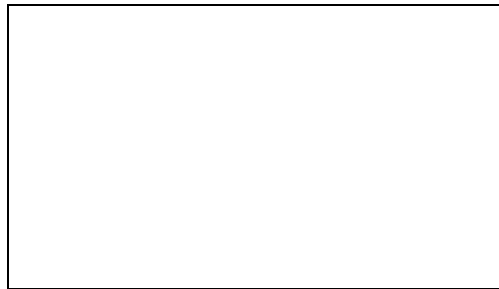


Figure 2.3: Extension of a spring

2.5.3 Anelasticity

The property of a solid in which deformation depends on the time rate of change of stress as well as on the stress itself. Characteristic exhibited by certain materials in which strain is a function of both stress and time, such that while no permanent deformations are involved, a finite time is required to establish equilibrium between stress and strain in both the loading and unloading directions. The term anelasticity is used to denote that property of metals in virtue of which strain is not a unique function of stress even at such low stress levels that no permanent set is observed.

2.5.4 Tensile Properties

Yield point.: If the stress is too large, the strain deviates from being proportional to the stress. The point at which this happens is the *yield point* because there the material yields, deforming permanently (plastically).

Yield stress: Hooke's law is not valid beyond the yield point. The stress at the yield point is called *yield stress*, and is an important measure of the mechanical properties of materials. The yield stress measures the resistance to plastic deformation.

The reason for plastic deformation, in normal materials, is not that the atomic bond is stretched beyond repair, but the motion of dislocations, which involves breaking and reforming bonds. Plastic deformation is caused by the motion of dislocations.

Tensile strength: When stress continues in the plastic regime, the stress-strain passes through a maximum, called the *tensile strength* (σ_{TS}), and then falls as the material starts to develop a *neck* and it finally breaks at the fracture point

2.5.5 True Stress and Strain

The concept of engineering stress treats the area under consideration as a constant (A_0). In reality however the area does not remain constant. And in the case of an axially loaded tensile bar, gradually decreases as the stress.

Instantaneous % of change in length of specimen in mechanical test. It is equal to the natural logarithm of the ratio of length at any instant to original length.

2.5.6 Elongation

The physical state and morphology of a polymer have a strong influence on its mechanical properties. A simple measure of the differences produced in mechanical behaviour is the elongation that occurs when a plastic is loaded (stressed) in tension. A glassy polymer such as polystyrene is quite stiff, showing a high ratio of initial stress to initial elongation.

2.5.7 Hardness

Hardness is the resistance of a material to localized deformation. The term can apply to deformation from indentation, scratching, cutting or bending. In metals, ceramics and most polymers, the deformation considered is plastic deformation of the surface. For elastomers and some polymers, hardness is defined at the resistance to elastic deformation of the surface. The lack of a fundamental definition indicates that hardness is not be a basic property of a material, but rather a composite one with contributions from the yield strength, work hardening, true tensile strength, modulus, and others factors. Hardness measurements are widely used for the quality control of materials because they are quick and considered to be nondestructive tests when the marks or indentations produced by the test are in low stress areas. There are a large variety of methods used for determining the hardness of a substance.

2.6 Thermal Analyses

2.6.1 Theory of thermal analyses

Thermal analysis includes a group of techniques where some physical property of the sample is monitored under controlled conditions with variation of temperature at a programmed rate. Thermal analysis is a branch of materials science where the properties of materials are studied as they change with temperature. Several methods are commonly used - these are distinguished from one another by the property which is measured:

- ❖ Differential thermal analysis (DTA): temperature difference
- ❖ Thermogravimetric analysis (TGA): mass change
- ❖ Differential scanning calorimetry (DSC): heat difference

2.6.2 Differential Thermal analysis

The DTA is a thermoanalytic technique, similar to differential scanning calorimetry. In DTA, the material under study and an inert reference are made to undergo identical thermal cycles, while recording any temperature difference between sample and

reference. This differential temperature is then plotted against time, or against temperature (DTA curve or thermogram). Changes in the sample, either exothermic or endothermic, can be detected relative to the inert reference. Thus, a DTA curve provides data on the transformations that have occurred, such as glass transitions, crystallization, melting and sublimation. The area under a DTA peak is the enthalpy change and is not affected by the heat capacity of the sample.

The DTA to study the structural and phase changes occurring both in solid in liquid materials during heat treatment. These changes may be dehydration, transition, decomposition, degradation temperatures, etc.

These differences of temperatures appear because of the phase transitions or chemical reactions in the sample involving the evolution of heat are known as exothermic reaction or absorption of heat known as endothermic reaction. The exothermic and endothermic reactions are generally shown in the DTA traces as positive and negative deviations respectively from a base line. So DTA offers a continuous thermal record of reactions in a sample. The areas under the bands or peaks of DTA spectra are proportional to the amount of heat absorbs or evolved from the sample under investigation, where temperature and sample dependent thermal resistance are the proportionality factors. Thus DTA is needed primarily for the measurement of transition temperature.

DTA Measurement Principle:

DTA involves heating or cooling a test sample and an inert reference under identical conditions, while recording any temperature difference between the sample and reference. This differential temperature is then plotted against time, or against temperature. Changes in the sample which lead to the absorption or evolution of heat can be detected relative to the inert reference.

Differential temperatures can also arise between two inert samples when their response to the applied heat-treatment is not identical. DTA can therefore be used to study thermal properties and phase changes which do not lead to a change in enthalpy. The baseline of

the DTA curve should then exhibit discontinuities at the transition temperatures and the slope of the curve at any point will depend on the microstructural constitution at that temperature.

The key features of a differential thermal analysis kit are as follows (Fig. 2.4):

1. Sample holder comprising thermocouples, sample containers and a ceramic or metallic block.
2. Furnace.
3. Temperature programmer.
4. Recording system.

The last three items come in a variety of commercially available forms and are not be discussed in any detail. The essential requirements of the furnace are that it should provide a stable and sufficiently large hot-zone and must be able to respond rapidly to commands from the temperature programmer. A temperature programmer is essential in order to obtain constant heating rates. The recording system must have a low inertia to faithfully reproduce variations in the experimental set-up.

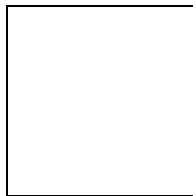


Figure 2.4: Schematic illustration of a DTA cell.

The sample holder assembly consists of a thermocouple each for the sample and reference, surrounded by a block to ensure an even heat distribution. The sample is contained in a small crucible designed with an indentation on the base to ensure a snug fit over the thermocouple bead. The crucible may be made of materials such as Pyrex, silica, nickel or platinum, depending on the temperature and nature of the tests involved. The thermocouples should not be placed in direct contact with the sample to avoid contamination and degradation, although sensitivity may be compromised.

2.6.3 Thermogravimetric analysis

TGA is a technique in which the mass of a substance is measured as a function of temperature while the substance is subjected to a controlled temperature programme. The record is the thermogravimetric or TG curve; the mass is plotted on the ordinate decreasing downwards and temperature (T) or time (t) on the abscissa increasing from left to right. This can be very useful to investigate the thermal stability of a material, or to investigate its behavior in different atmospheres (e.g. inert or oxidizing). It is suitable for use with all types of solid materials, including organic or inorganic materials.

The TGA is a special branch of thermal analysis, which examines the mass change of a sample as a function of temperature in the scanning mode or as a function of time in the isothermal mode. Not all thermal events bring about a change in the mass of the sample (for example melting, crystallization or glass transition), but there are some very important exceptions which include absorption, sublimation, vaporization, oxidation, reduction and decomposition. The TGA is used to characteristics the decomposition and thermal stability of materials under a variety of conditions, and to examine the kinetics of the physico-chemical process occurring in the sample. Sample weight changes are measured.

Principle: The sample balance beam and reference balance beam are independently supported by a driving coil/pivot. When a weight change occurs at the beam end, the movement is conveyed to the opposite end of the beam via the driving coil/pivot, when optical position sensors detect changes in the position of a slit. The signal from the optical position sensor is sent to the balance circuit. The balance circuit supplies sufficient feedback current to the driving coil to the sample side and current running to the driving coil on the reference side is detected and converted into weight signals.

It is usual to control the temperature in a predetermined way- either by a continuous increase or decrease in temperature at a constant rate (linear heating/cooling) or by carrying out a series of determinations at different temperatures.

Melting and degradation temperatures of the samples were monitored by a DTA and TGA (Seiko-Ex-STAR-6300, Japan). The measurements using DTA and TGA were carried out from 30 to 700 °C at a heating rate of 20 °C min⁻¹ under nitrogen gas flow.

While the DTA traces give the melting and degradation temperatures as determined from the exotherm versus temperature curves, the TGA runs exhibit the loss of weight with temperature.

2.6.4 Differential scanning calorimetry

The DSC is a thermoanalytical technique in which the difference in the amount of heat required to increase the temperature of a sample and reference is measured as a function of temperature. Both the sample and reference are maintained at nearly the same temperature throughout the experiment. Generally, the temperature program for a DSC analysis is designed such that the sample holder temperature increases linearly as a function of time. The reference sample should have a well-defined heat capacity over the range of temperatures to be scanned.

Detection of phase transitions

The basic principle underlying this technique is that when the sample undergoes a physical transformation such as phase transitions, more or less heat will need to flow to it than the reference to maintain both at the same temperature. Whether less or more heat must flow to the sample depends on whether the process is exothermic or endothermic. When a solid sample melts to a liquid it will require more heat flowing to the sample to increase its temperature at the same rate as the reference. This is due to the absorption of heat by the sample as it undergoes the endothermic phase transition from solid to liquid. Likewise, as the sample undergoes exothermic processes (such as crystallization) less heat is required to raise the sample temperature. By observing the difference in heat flow between the sample and reference, differential scanning calorimeters are able to measure the amount of heat absorbed or released during such transitions. DSC may also be used to observe more subtle phase changes, such as glass transitions. It is widely used in industrial settings as a quality control instrument due to its applicability in evaluating sample purity.

2.6.5 What is Scanning Electron Microscopy

A typical Scanning Electron Microscopy (SEM) instrument, showing the electron column, sample chamber, EDS detector, electronics console, and visual display monitors.

The SEM uses a focused beam of high-energy electrons to generate a variety of signals at the surface of solid specimens. The signals that derive from electron-sample interactions reveal information about the sample including external morphology (texture), chemical composition, and crystalline structure and orientation of materials making up the sample. In most applications, data are collected over a selected area of the surface of the sample, and a 2-dimensional image is generated that displays spatial variations in these properties. Areas ranging from approximately 1 cm to 5 microns in width can be imaged in a scanning mode using conventional SEM techniques (magnification ranging from 20X to approximately 30,000X, spatial resolution of 50 to 100 nm). The SEM is also capable of performing analyses of selected point locations on the sample; this approach is especially useful in qualitatively or semi-quantitatively determining chemical compositions (using EDS), crystalline structure, and crystal orientations (using EBSD). The design and function of the SEM is very similar to the EPMA and considerable overlap in capabilities exists between the two instruments.

Fundamental Principles of Scanning Electron Microscopy

Accelerated electrons in an SEM carry significant amounts of kinetic energy, and this energy is dissipated as a variety of signals produced by electron-sample interactions when the incident electrons are decelerated in the solid sample. These signals include secondary electrons (that produce SEM images), backscattered electrons (BSE), diffracted backscattered electrons (EBSD that are used to determine crystal structures and orientations of minerals), photons (characteristic X-rays that are used for elemental analysis and continuum X-rays), visible light (cathodoluminescence--CL), and heat. Secondary electrons and backscattered electrons are commonly used for imaging samples: secondary electrons are most valuable for showing morphology and topography on samples and backscattered electrons are most valuable for illustrating contrasts in composition in multiphase samples (i.e. for rapid phase discrimination). X-ray generation is produced by inelastic collisions of the incident electrons with electrons in discrete orbitals (shells) of atoms in the sample. As the excited electrons return to lower

energy states, they yield X-rays that are of a fixed wavelength (that is related to the difference in energy levels of electrons in different shells for a given element). Thus, characteristic X-rays are produced for each element in a mineral that is "excited" by the electron beam. SEM analysis is considered to be "non-destructive"; that is, x-rays generated by electron interactions do not lead to volume loss of the sample, so it is possible to analyze the same materials repeatedly.

2.7 Dielectrics

The study of dielectric properties is concerned with the storage and dissipation of electric and magnetic energy in materials. It is important to explain various phenomena in electronics, optics, and solid-state physics. A dielectric is an electrical insulator that may be polarized by an applied electric field. When a dielectric is placed in an electric field, electric charges do not flow through the material, as in a conductor, but only slightly shift from their average equilibrium positions causing dielectric polarization. Because of dielectric polarization, positive charges are displaced toward the field and negative charges shift in the opposite direction. This creates an internal electric field that partly compensates the external field inside the dielectric. If a dielectric is composed of weakly bonded molecules, those molecules not only become polarized, but also reorient so that their symmetry axis aligns to the field. Although the term "insulator" refers to a low degree of electrical conduction, the term "dielectric" is typically used to describe materials with a high polarizability. The latter is expressed by a number called the dielectric constant. A common, yet notable example of a dielectric is the electrically insulating material between the metallic plates of a capacitor. The polarization of the dielectric by the applied electric field increases the capacitor's surface charge.

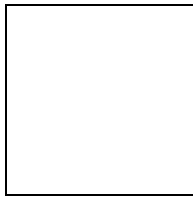
2.7.1 Dielectric constant

The dielectric constant is the ratio of the permittivity of a substance to the permittivity of free space. It is an expression of the extent to which a material concentrates electric flux, and is the electrical equivalent of relative magnetic permeability.

As the dielectric constant increases, the electric flux density increases, if all other factors remain unchanged. This enables objects of a given size, such as sets of metal plates, to hold their electric charge for long periods of time, and/or to hold large quantities of charge. Materials with high dielectric constants are useful in the manufacture of high-value capacitors.

2.7.2 Dielectric Loss

Capacitors are used for a wide variety of purposes and are made of many different materials in many different styles. For purposes of discussion we will consider three broad types, that is, capacitors made for ac, dc, and pulse applications. The ac case is the most general since ac capacitors will work (or at least survive) in dc and pulse applications, where the reverse may not be true. It is important to consider the losses in ac capacitors. All dielectrics (except vacuum) have two types of losses. One is a conduction loss, representing the flow of actual charge through the dielectric. The other is a dielectric loss due to movement or rotation of the atoms or molecules in an alternating electric field. Dielectric losses in water are the reason for food and drink getting hot in a microwave oven. One way of describing dielectric losses is to consider the permittivity as a complex number, defined as



where

ϵ' = ac capacitance

ϵ'' = dielectric loss factor

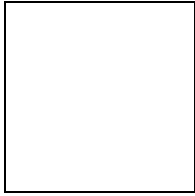
δ = dielectric loss angle

Dielectric loss tangent is calculated by the following formula

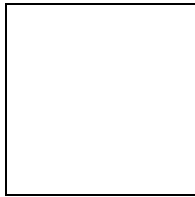
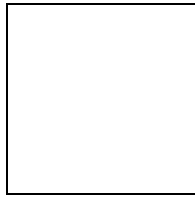
$$\tan \delta = \frac{G_p}{2\pi f C_p}$$

2.7.3 Debye relaxation

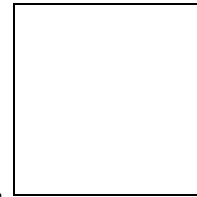
Debye relaxation model was named after the chemist Peter Debye. Debye relaxation is the dielectric relaxation response of an ideal, noninteracting population of dipoles to an alternating external electric field. It is usually expressed in the complex permittivity



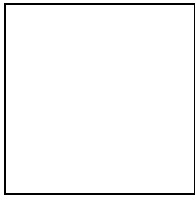
of a medium as a function of the field's frequency ω :



where



where



is the static, low frequency permittivity, and τ is the characteristic relaxation time of the medium.

3.1 Raw Materials	44
3.2 Equipment for Sample Preparation	44
3.2.1 Fabricated extrusion machine	44
3.3 Composite Preparation Procedure	46
3.4 Mechanical Testing	46
3.5 Scanning Electron Microscopy	47
3.6 Methods of Measuring Mechanical Properties	47
3.6.1 Tensile Test	48
3.6.2 Micromechanical testing	48
3.7 Thermal Testing	49
3.8 AC Electrical Measurements	49
3.8.1 Instruments	49
3.8.2 AC measurement procedure	52

3.1 Raw Materials

PP and TiO₂ was purchased from local market. Different sets of composites were prepared by mixing 10, 20, 30, 40 and 50 wt% TiO₂ with Polypropylene (PP). Granular-shaped iPP ($M_w=184.7 \text{ kg mol}^{-1}$) and TiO₂ powder of particle size less than 0.2 mm were purchased from BASF, Germany and local market, respectively.

3.2 Equipment for sample preparation

3.2.1 Fabricated Extrusion Machine

Extrusion is the process of pushing the heated billet or slug of polymers, composites, etc, through an orifice. It was a faster process. The products have good tolerances and have good surface finish. Complex shapes can be easily extruded. The whole set-up is shown in Figure 3.1. Various parts of the fabricated extrusion machine are described below:



Figure 3.1: The Extrusion Machine setup in the laboratory

(b) The Extruder Screw

The extrusion screw is the most important element of extrusion machine. The length of the screw is divided into three zones: feed, compression and metering. The purpose of feed zone is to pick up the mixed batch of PP and TiO_2 from the feed hopper and to move them into the main length of the extruder. In the compression zone the loosely packed mixture is compacted and softened to produce a continuous stream of molten composite from the compression zone and feeds it at a controlled through the dice. The screw is driven by an alternating current motor; Continuous variation of screw speed is normally required. A screw of smaller diameter must be operated at a faster speed than one of the larger diameter. Speeds of operation range will below 100 rpm to above 100 rpm.

The fabricated extrusion machine set up in the laboratory has the following specifications for the extruder screw.

(c) The barrel

Barrel surrounds the screw resisted the pressure generated by the screw, which may be as high as 6000 PSI. Usually; the length of the barrel was electrically heated by band heaters around it.

Specifications of the barrel are as follows:

- (a) Length of the barrel = 0.88 meter
- (b) Inner diameter = 0.0112 meter
- (c) Outer diameter = 0.0135 meter

(d) Profile Dices

Dices for profiles such as moldings, counter edging rods etc, have an orifice of the approximate shape size of the required contour. The final shape developing outside the dice as the material wraps and shrinks or expands. By trial of extruder the shape of the dice orifice is modified as required. The size and shape of an extended profile can also be changed by altering the extrusion speed and the rate of cooling after the composite leaves the dice. Usually the dice orifice is made oversize.

(e) Cooling and Take off Equipment

As the fluid composites leave the dice, it must be supported by fixture usually called a sizing plate, to retain the desired shape through period when the materials pools. By changing the speed of the take of equipment it possible to control the dimension of the contour, a faster take of will produce greater draw down.

f) Breaker and Screen Pack

At the end of the screw the plastic is delivered through a breaker plate and screens to the die. The breaker plate is a thick plate drills holes about 1/8 to 1/4 inches in diameter. The screen pack consists of several layers of stainless wire screen which stain out foreign material and unmated granular substances.

g) Heaters

The fabricated machine has three heater situated at a distance 0.09 meter from each other. The heaters can heat the barrel up to 573 K.

3.3 Composite Preparation Procedure

Five different composites were prepared with different mixture ratio of PP and TiO₂. At first, five batches of mixture with 0.10, 0.20, 0.30, 0.40 and 0.50 kg of TiO₂ in 1 kg PP were made. A pure PP sample was also produced.

A neat iPP sample and the mixtures of iPP and 10, 20, 30, 40 and 50 wt% TiO₂ were extruded by a locally fabricated extruder machine. The extruder has 3 heating zones with blending temperature profiles of 220, 230 and 240 °C and a screw rotating speed of 100 rpm. During preparation of extrusion molded (EM) samples, molten extrudates were directly cast in a circular-shaped die. On the other hand, a cylindrical die having 0.008 m diameter and 0.05 m length was used to cast rod-shaped extrudates emerging from the extruder. These molten extrudates were cooled to solid-state and then cut into pieces, which were once molded in a dumbbell-shaped mold with a load of 100 kN at 180 °C by compression molding machine. Molten materials were kept at 180 °C for 10 min before melt-compressed, and then slowly cooled to room temperature. After that, this technique was repeated to each sample employing the same conditions to obtain extrusion cum compression-molded (ECM) samples. Thus, EM and ECM samples of varying thicknesses (0.002–0.0025 m) were obtained and subjected to characterization by the following techniques to observe the effect of molding.

3.4 Mechanical testing

Stress-strain behavior tensile strength (TS) and percentage of elongation-at-break [EB(%)] or breaking strain of the composites were measured by a universal testing machine shown in figure 3.2 [Hounsfield UTM 10KN; ASTM D-638–98] at a crosshead speed of 0.002 m.min⁻¹, keeping a gauge length of 0.05 m. Five samples of each composition were used in the mechanical testing. The average TS and EB (%) values of the composites were evaluated using the data of all five samples. For this purposes, stress-strain curve was plotted only for one of the five samples of each composition.

3.5 Scanning Electron Microscopy: Surface Morphology

The surface morphology of the pure iPP and composites sample with 10, 20, 30, 40 wt% TiO₂ was studied by a scanning electron microscope (Philips XL 30, Netherlands) with a maximum operating voltage of 10 kV of the apparatus from MME department of BUET. The sample surface was coated with a thin gold layer by a sputtering prior to SEM measurement.

3.6 Methods of Measuring Mechanical Properties

The mechanical properties of prepared composites were studied by the following equipment and testing procedure. Figure 3.2 shows the Hounsfield UTM 10KN (H10KS) used for test of tensile strength.



Figure 3.2: Hounsfield Universal Testing Machine (UTM)

Figure 3.3: Different views of the tensile test specimen

3.6.1 Tensile test

(a) **Tensile Strength** = Applied load/Cross sectional area of the load bearing area

(b) **Tensile Strain:** It is calculated according to ASTM D-638M – 91a.

$$\text{Tensile Strain} = \text{Extension (mm)} / 50 \text{ (mm)}$$

3.6.2 Micromechanical Testing

To measure the microhardness (H) from the residual impression on the sample on the sample surface, a software controlled Vicker's square-based diamond indenter with indentation time of 15s (Shimadzu, Japan) was employed. Loads of 0.245, 0.490 and 0.980 N was used to derive a load independent value of H in MPa by the following relation [28]:

$$H = K \frac{P}{d^2}$$

Where

K → Geometrical factor

P → Applied load in Newton

d → Indentation diagonal in meter

3.7 Thermal Testing

Melting, degradation temperatures and mass/wt loss of the samples were monitored by a differential thermal analyzer (DTA) and thermogravimetric analyzer (TGA) [Seiko-ExSTAR-6300, Japan]. The measurements using DTA and TGA were carried out from 30 to 700 °C at a heating rate of 20 °C min⁻¹ under nitrogen gas flow. While the DTA traces give the melting and degradation temperatures as determined from the exotherm versus temperature curves, the TGA runs exhibit the loss of weight with temperature.

Differential scanning calorimetry (DSC) was carried out in the temperature range of -50 to 50 °C using a DSC-Q10 (TA, USA) apparatus, purged with nitrogen gas and chilled with liquid nitrogen. Each sample was heated at a heating rate of 10 °C/min.

3.8 AC Electrical Measurements

Followings are the equipments used in the AC electrical measurement procedure.

3.8.1 Instruments

(a) LF Impedance analyzer

Samples in the form of disc structure were prepared for AC measurement. The ac measurement was performed in the frequency range from 100 to 1×10^6 Hz and temperature range 300-375 K, by an Agilent 4192A LF Impedance analyzer, 5Hz-13MHz (Agilent Technologies Japan Ltd, Japan). The temperature was recorded by a Chromel-Alumel thermocouple placed very closed to the sample which was connected to a Keithley 197A digital microvoltmeter (DMV). All measurements were carried out in a vacuum of about 1.33 Pa. Photographs of the LF Impedance analyzer and AC measurement system are shown in Fig. 3.4.



Figure 3.4 Arrangement of AC measurement

(b) Oil Rotary Pump

An oil rotary pump was to evacuate the specimen chamber. A pressure of about 10^{-2} torr can be attained using this pump.



Figure 3.5: Photograph of oil rotary pump.

(c) Keithley Microvolt Meter

A digital Keithley autoranging microvolt meter MVM (Model 197 A) was used for the measurement of e.m.f. across a Cr – Al thermocouple attached to the specimen.

(d) Specimen Chamber

Specimen chamber is designed and fabricated in the laboratory with the help of university workshop. It consists of two main parts, mainly the stainless steel tube and the sample holder. A stainless steel tube having inner diameter of 0.045 m and length 0.24 m is used. The lower end of the tube is closed by welding a circular piece of stainless steel. At the top of the tube one flat stainless steel sheet ($0.092 \times 0.09\text{m}^2$); with a circular hole (diameter 0.045 m) at its center is welded. Another stainless with a hole of the same dimension is welded to a stainless steel tube of diameter 0.045 m and of length 0.24 m. A O – ring is placed in between the two stainless steel sheets. This prevents the air leakage when it is evacuated. The upper portion can be fixed to the lower portion by screws. The top opening is closed tightly with teflon stopper. Two copper leads (electrodes) which hold the specimen holder and a Cr-Al thermocouple are inserted through this teflon stopper. A thick layer of mica sheet is placed on

to the inside wall and bottom of the stainless steel tube for electrical insulation. The distance between the leads is about 0.014 m. This is a side tube welded to the main stainless steel tube which acts as an outlet of the chamber. A rotary vacuum pump is connected to the chamber through the side tube with the help of rubber tube. By this pump a pressure of about 110^{-2} torr can be obtained. Required temperature in the chamber can be maintained by a heating tape which is wrapped outside the steel tube and its temperature is controlled by a variable transformer. Sample holder is a spring system.

(e) Heating Tape

A heating tape (ISOPAD LTD BOREH AMWOOD, HERTS, ENGLAND) was used to heat the specimen chamber. It is about 1.75m long and .03m width tape. It can be wrapped around the specimen chamber easily.

(f) Variac

A Yamabishi volt-slider (Type SS-260-10 NO. 38 – 1) was connected to the heating tape.



Figure 3.5 Photograph of the specimen holder

3.8.2 AC measurement procedure

The silver paste coated sample was placed in between the electrodes inside the specimen chamber. The chamber was evacuated using a rotary vacuum pump to about 10^{-2} torr. The sample was connected to the LF impedance Analyzer. The values of capacitance and conductance were recorded at different frequencies and at different temperatures. The dielectric constant, ac conductivity and loss tangent were calculated by using the following equations.

$$\varepsilon' = \frac{C_p d}{\varepsilon_0 A}$$

$$\sigma_{ac} = \frac{G_p d}{A}$$

$$\tan \delta = \frac{G_p}{\omega C_p} = \frac{G_p}{2\pi f C}$$

Where,

C_p =Capacitance of the sample

G_p = Conductance

A = Cross-sectional area of the sample

d = Sample thickness

$\omega=2\pi f$ is the angular frequency.

CHAPTER 4 RESULTS AND DISCUSSION

4.1 Surface Morphology	56
4.2 Mechanical Properties	59
4.3 Micromechanical Properties	61
4.4 Thermal Analysis	62
4.5 AC Electrical Studies	
4.5.1 Variation of ac conductivity on frequency at different temperatures	65
4.5.2 Dependence of dielectric constants on frequency at different temperatures	67
4.5.3 Variation of loss tangent with frequency and temperature	70

Results and Discussion

4.1.1 Surface Morphology

SEM micrographs provide us useful information about the microvoids or holes that increase in the composites with increasing the amount of filler. The reason of the presence of more holes may be for the development of interface around the particles due to their incompatibility with iPP matrix.

Fig. 4.1 represents the SEM micrographs of the extrusion molded (EM) and extrusion cum compression molded (ECM) iPP sample and composites with 20 and 40 wt% TiO₂ content. Clearly, the iPP sample shows the smoothest surface in comparison to other two composites, and the composite surface of 20 wt% TiO₂ seems to be slightly smoother and becomes less white than that of 40 wt% filler. The composite of 40 wt% TiO₂ contains more agglomerates or larger particles, which seem to form lumps on the surface, than the composite of 20 wt% TiO₂. Increasing TiO₂ content develops slight roughness and whiteness on the ECM composite surfaces but does not show any noticeable gap or sharp boundary between filler and polymer matrix. Gaps are significantly notable in the EM composite of 40 wt% TiO₂.

The surface fatigue has been observed for all fractured samples by the SEM. Figure 4.2 represents the SEM micrographs of the neat iPP and the composites surface, fractured at room temperature (30 °C) through tensile test. Small particles are seen to disperse inhomogeneously in the iPP matrix in the composite samples. While the surface of the neat iPP (Fig. 4.1a) shows a few cracks, terraces and voids, a considerable amount of voids appear in the composites indicating different fracture processes in the neat iPP and the composites. The size of the particles, as measured by the SEM, ranges from several hundred nanometers to micrometers, whereas that of the voids is of the order of microns. These observed voids are created around filler particles during fracture by the application of tensile force. However, a few voids on the surface of neat iPP may originate from the existing impurity during polymerization of iPP. The number of voids is found to increase with the increase of TiO₂ particles.

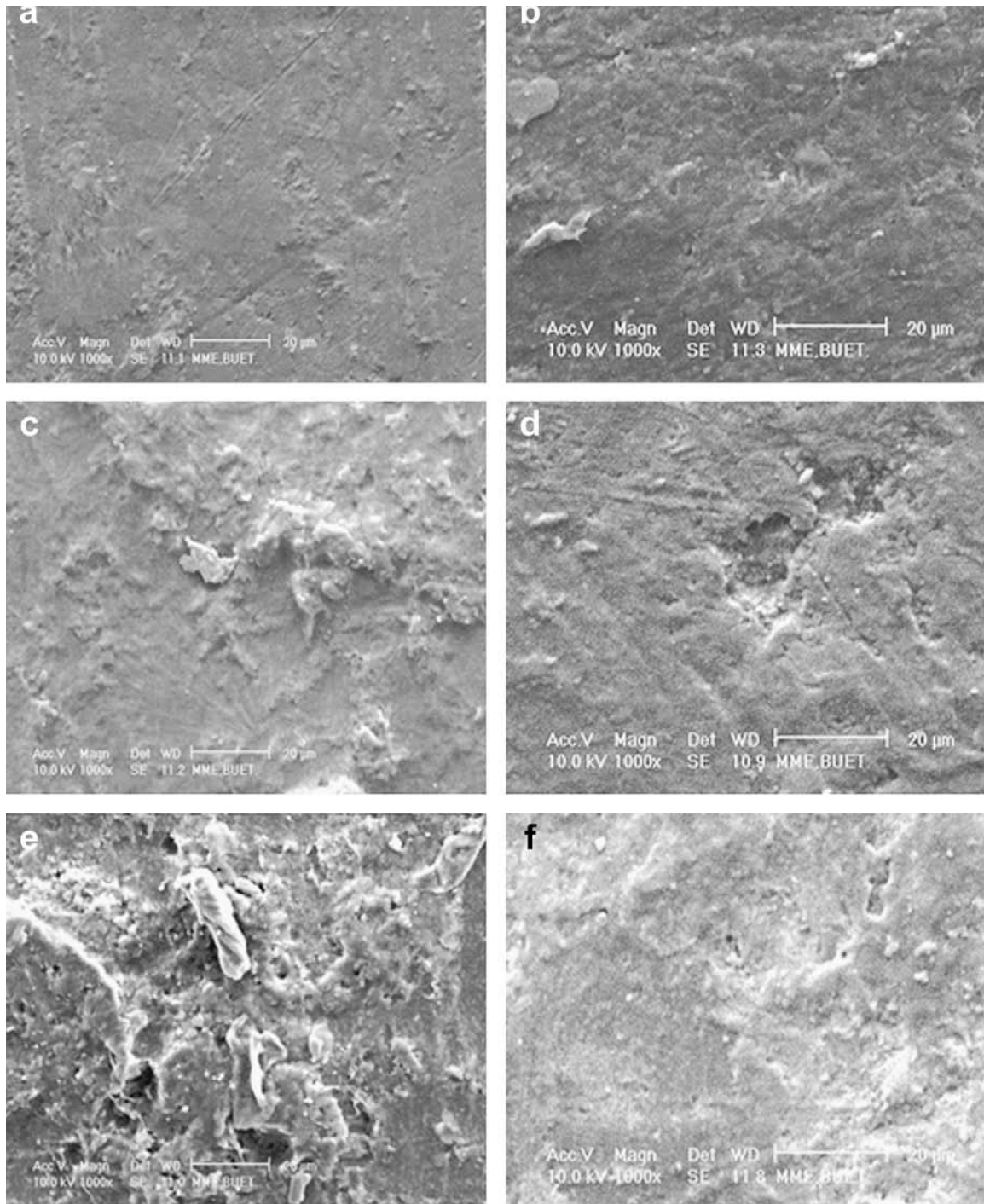


Figure 4.1: SEM micrographs of the extrusion-molded samples [(a)–(c)] and the extrusion cum compression-molded samples [(d)–(f)]: (a) and (d) neat iPP, (b) and (e) iPP 20 wt% TiO₂ and (c) and (f) iPP 40 wt% TiO₂.

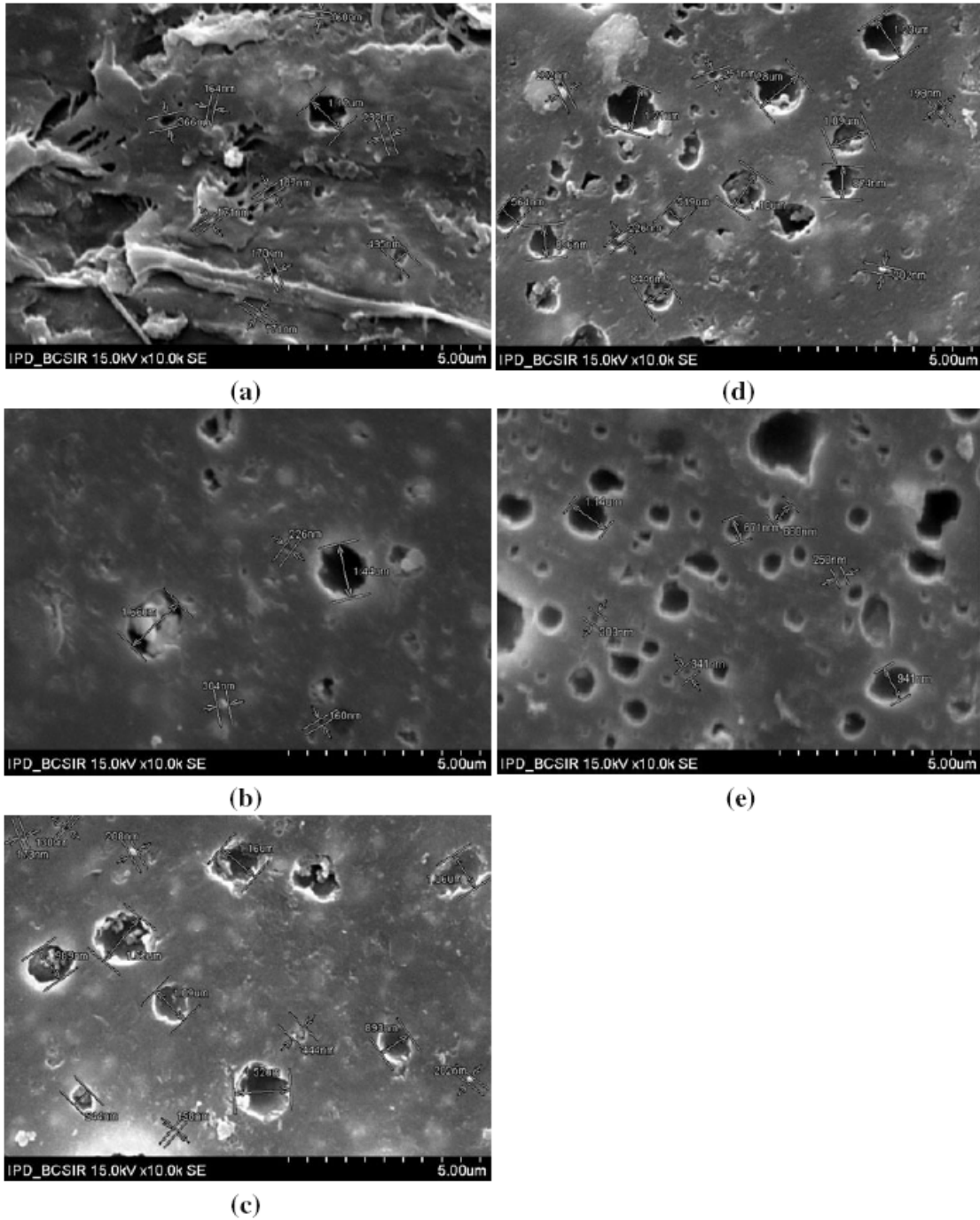


Figure 4.2 SEM micrographs of the (a) iPP sample, (b) 10 (c) 20 (d) 30 and (e) 40 wt% TiO₂ loaded composites after fracture through the tensile test

4.2 Mechanical properties (Tensile Properties)

Figure 4.3 illustrates stress (σ) versus strain (ϵ) curves for neat iPP and the composites processed with various amount of TiO_2 . For all samples, the σ - ϵ curves first show a linear variation followed by a gradual increase to a level-off value and eventually ceases, indicating the break of the samples.

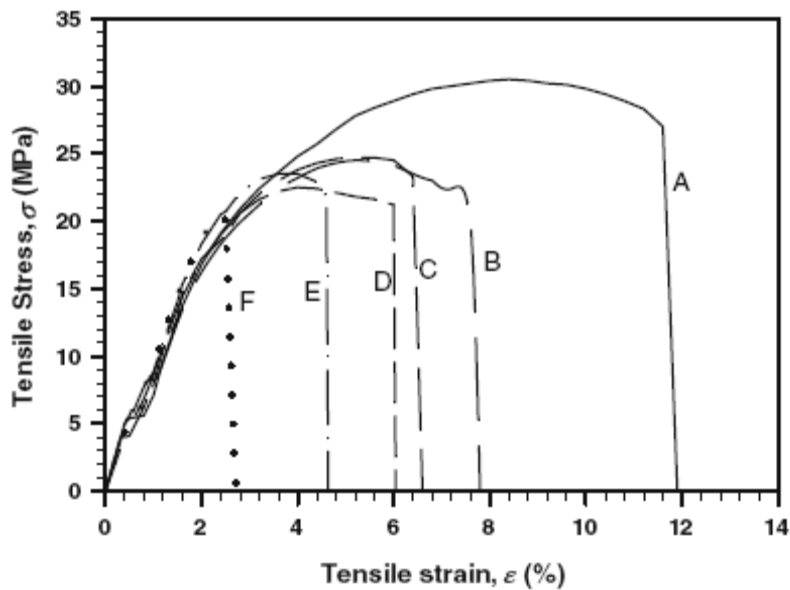


Figure 4.3: Tensile stress versus strain of the neat sample and composites with various concentrations of TiO_2 (A: neat iPP, B: 10% wt% TiO_2 , C: 20% wt% TiO_2 , D: 30% wt% TiO_2 , E: 40% wt% TiO_2 , F: 50% wt% TiO_2)

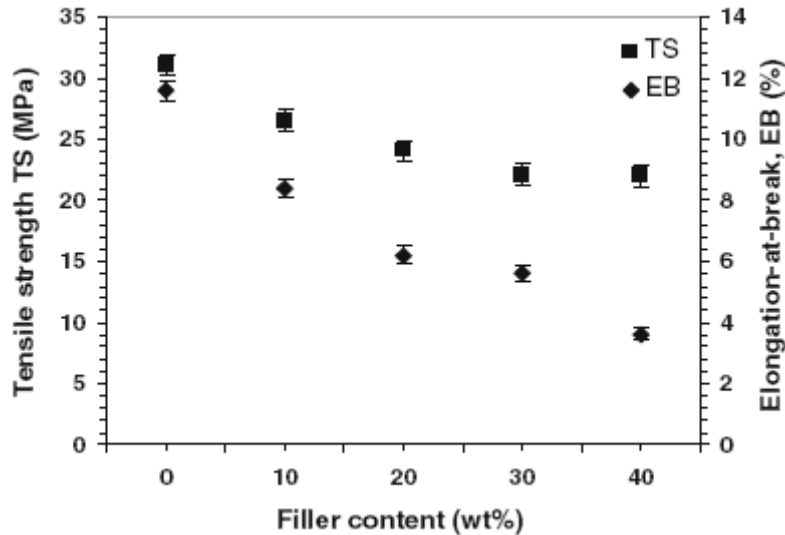


Figure 4.4: Variation of tensile strength and elongation-at- break (%) of the iPP/TiO₂ composites with increasing filler content

The patterns of the σ - ϵ plots vary depending on the amount of filler content. In addition, the σ - ϵ variations obtained at low strains are apparently indistinguishable. The variations of TS and EB (%) with TiO₂ content are shown in Fig. 4.4. The TS and EB (%) of neat iPP are comparatively high and then decrease gradually with the increase of TiO₂ content. These changes of mechanical properties may be related to the changes of internal structures of the samples.

The TS basically expresses the ability for polymer chains to slip past each other. The more difficult is the slippage of chain molecules, the greater is the TS. The neat iPP exhibits both crystalline and amorphous regions [28]. Due to the presence of more crystalline region in the neat iPP, its TS value is higher. Furthermore, for the presence of amorphous regions, the long polymer chains have space to orient themselves in the sample to form oriented crystals. Due to this reason, the neat iPP shows higher EB(%). As increasing filler content changes crystallinity and crystallite size, the TS and EB(%) gradually decrease.

In a fairly large number of reports, it is found that the particle size plays a dominant role in structure and properties of polymeric composites [29–36]. A low loading of filler content and the nano-particles exhibit higher crystallization of iPP with improved mechanical, thermal and electrical properties of the final composites. Contrary to this, a high loading of filler may result in a larger probability of particle agglomeration. In neat iPP, the stress can continuously be concentrated throughout the sample if it is stretched, whereas in the composites, the discontinuity of stress transfer increases with the higher amount of filler or agglomerate. Due to the decrease in crystallinity and restriction to chain mobility in the composites, the stress concentration at the particle interface can develop local crazes or cracks, which propagate in all directions, resulting in voids. Increasing interface area around particles affects to fracture the composites at a relatively low stress and strain. Thus, the TS and EB (%) decrease with increase of particles.

4.3 Micromechanical Properties

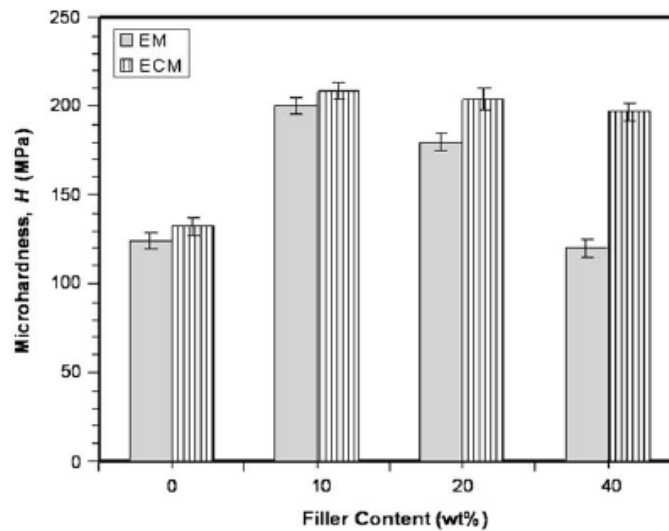


Figure 4.5: Change of microhardness at various concentrations of filler for both extrusion molded and extrusion cum compression molded samples

The change of microhardness against the amount of filler for both EM and ECM samples is illustrated by bar diagrams in Fig. 4.5. The H values are observed to be about 130 MPa and 120 MPa for the ECM and EM neat iPP sample, respectively. After inclusion of

TiO₂, the H increases gradually and then becomes to a level-off value of about 200 MPa with the increase of filler content for ECM samples. Evidently, the H values are lower for the EM samples than the ECM ones; especially much lower in case of 40 wt% filler. During indentation, both elastic and plastic deformations occur in the sample for the application of a load. Removal of the load causes a residual impression on the sample surface that exists due to the plastic deformation in the material. Therefore, if holes, cavities, crack and gaps between particles or crystallites, etc. defects are present on sample surface, they will generally result in higher diagonal length that corresponds to lower microhardness value. However, observed results for ECM samples show higher H values with the increase of particle content and clarify a good adhesion between filler and polymer matrix.

4.4 Thermal Analysis

The DTA and TGA curves of the neat iPP sample and composites of 10, 20 and 40 wt% TiO₂ content are presented in Fig. 4.6 (a) and (b), respectively. Each DTA run of the samples investigated shows two endothermic peaks that represent melting temperatures (T_m) at 169, 167, 163 and 167 °C and thermal degradation temperatures (T_d) at 435, 437, 448, 462 °C. While the melting peak of the neat iPP sample is sharp, the TiO₂-loaded composites rather show diffuse melting peaks along with a shift of peaks towards lower temperatures. Table 4.1 includes the values of T_m and T_d for both EM and ECM samples, indicating a clear difference of thermal properties of them as influenced by processing conditions. The TGA curves exhibit the weight loss of the samples with increasing temperature. The onset of this weight-decrease depends on TiO₂ content and is found to be increasing from 350 °C to higher values with increasing particle content. However, it is a common practice to consider the degradation temperature at 50% weight loss of the sample as an indicator for structural destabilization [36, 37]. Analysis shows that the neat sample is seen to be stable up to 416 °C, whereas 10, 20 and 40 wt% TiO₂-loaded samples show the thermal stability at higher temperatures of 429, 440 and 450 °C,

respectively (Fig. 4.6 (b)). Such increase of thermal stability in copperfilled low-density polyethylene and talc-filled polypropylene was observed by Luyt et al. [4] and Zhou et al. [5].

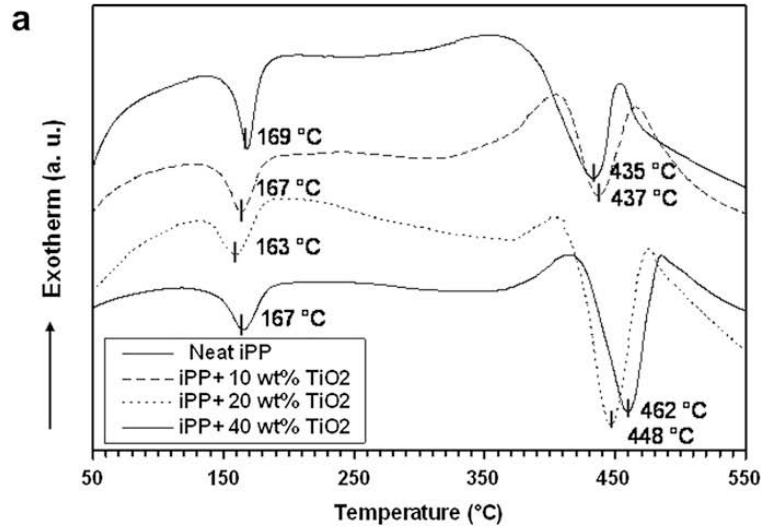


Figure 4.6(a): DTA thermograms of the extrusion cum compression molded neat iPP sample and iPP/TiO₂ composites having various contents of TiO₂.

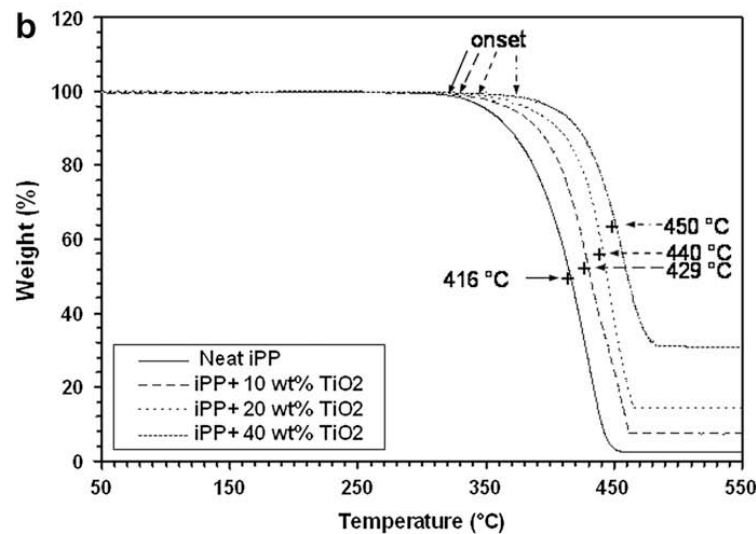


Figure 4.6(b): TGA thermograms of the extrusion cum compression molded neat iPP sample and iPP/TiO₂ composites having various contents of TiO₂.

Table 1
Melting and degradation temperatures (T_m and T_d) and resistivity (ρ) measured at 30 °C for both extrusion-molded and extrusion cum compression-molded samples.

Fabrication routes	Samples	Properties		
		T_m (°C)	T_d (°C)	ρ (ohm m)
EM	Neat iPP	168 ± 2.0	434 ± 2.7	7.13×10^8
	iPP + 10 wt% TiO ₂	166 ± 2.3	436 ± 3.2	6.45×10^8
	iPP + 20 wt% TiO ₂	166 ± 2.4	422 ± 2.8	6.11×10^8
	iPP + 40 wt% TiO ₂	167 ± 2.8	437 ± 3.1	6.62×10^8
ECM	Neat iPP	169 ± 1.9	435 ± 2.2	3.73×10^8
	iPP + 10 wt% TiO ₂	167 ± 2.1	437 ± 2.2	2.10×10^8
	iPP + 20 wt% TiO ₂	163 ± 2.1	448 ± 2.1	1.57×10^8
	iPP + 40 wt% TiO ₂	167 ± 2.3	462 ± 2.4	0.80×10^8

Table 4.1

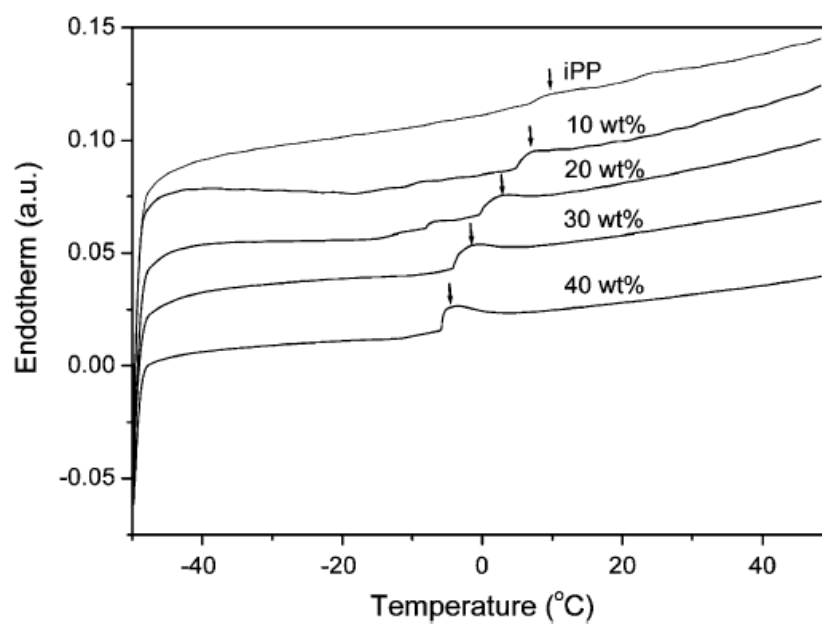


Figure 4.7: DSC curves showing the glass transition temperatures of the composites with different filler concentrations+

The glass transition temperatures (T_g) of all the samples investigated are presented in Fig. 4.7. The T_g value of neat iPP is observed to be at around 10 °C. This value is in agreement with the reported value [38]. The T_g values obtained for the neat iPP and the composites are recorded in Table 1. After inclusion of TiO_2 , the T_g decreases with the increase of filler content. This fact indicates a toughening behavior of the composites due to filler inclusion. Due to softening of the composites, the observed decrease of tensile strength and microhardness of the composites with the filler content is reasonable. The toughening behavior of iPP and high density polyethylene filled with calcium carbonate is also reported in the literature [39, 40].

4.5 AC electrical properties

4.5.1 Variation of ac conductivity on frequency at different temperatures

The measured values of the conductance and capacitance were used to calculate the ac conductivity, dielectric constant and loss tangent of the samples with different filler contents. Figure 4.8 [(a) - (d)] shows the dependence of ac conductivity on frequency of the iPP/ TiO_2 composites for different TiO_2 content at different temperatures. It observed from the figures that the conductivity increases with the increase of frequency but very weakly dependent on temperature.

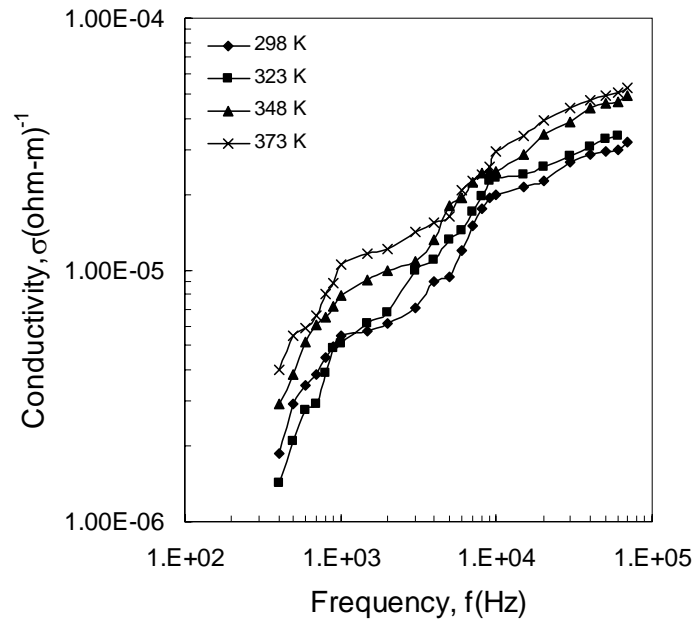


Figure 4.8 (a) Dependence of ac conductivity on frequency for iPP/TiO₂ composite with 10% TiO₂ at different temperatures.

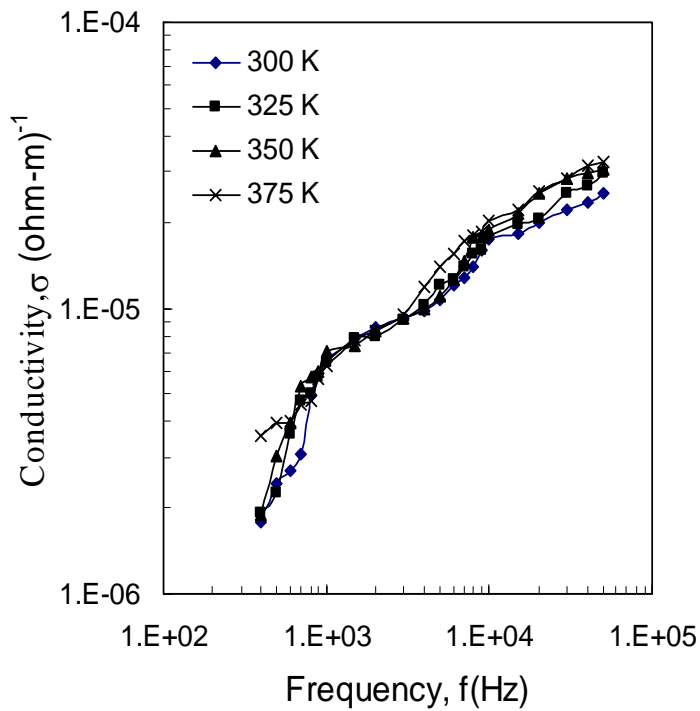


Figure 4.8 (b) Dependence of ac conductivity on frequency for iPP/TiO₂ composite with 20% TiO₂ at different temperatures.

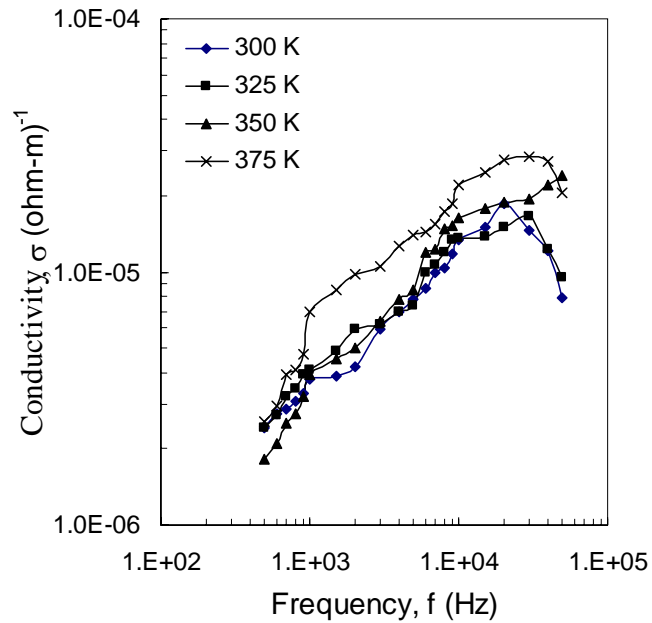


Figure 4.8 (c) Dependence of ac conductivity on frequency for iPP/TiO₂ composite with 30% TiO₂ at different temperatures.

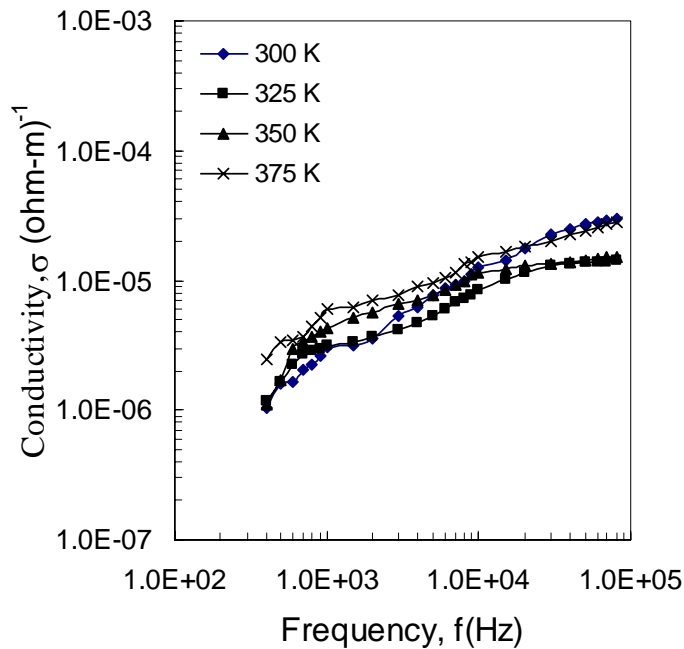


Figure 4.8 (d): Dependence of ac conductivity on frequency for iPP/TiO₂ composite with 50% TiO₂ at different temperatures.

4.5.2 Variation of dielectric constant on frequency at different temperatures

Figures 4.9 (a) - (e) show the variation of dielectric constant with frequency at temperatures 300, 325, 350 and 375 K. From the plots it is observed that the dielectric constant decreases with the increase in frequency and not much dependent on temperature. As the frequency increases the dipoles in the composite can not follow the field and thus lag behind the applied field. So the value of the dielectric constant decreases with the increase of frequency. The value of the dielectric constant becomes more or less uniform above 100 kHz frequency.

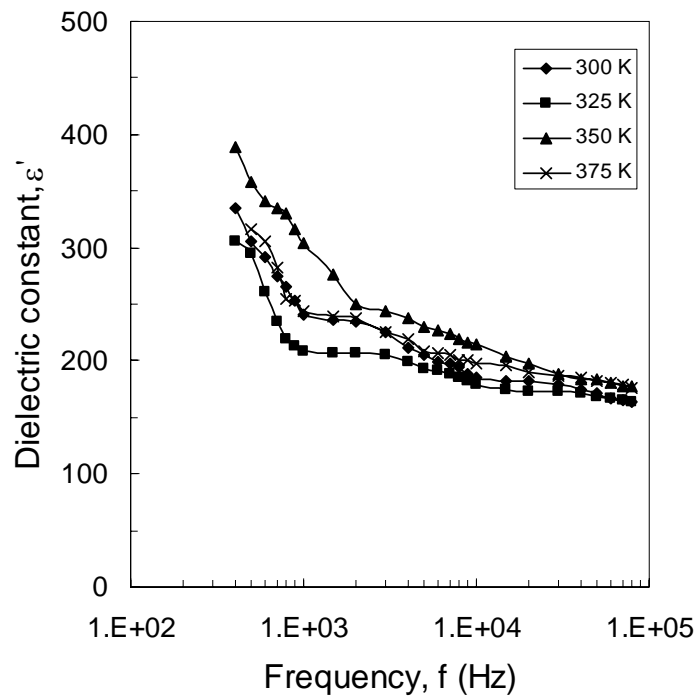


Figure 4.9 (a) Variation of dielectric constant with frequency for iPP/TiO₂ composite with 10 % TiO₂ at different temperatures.

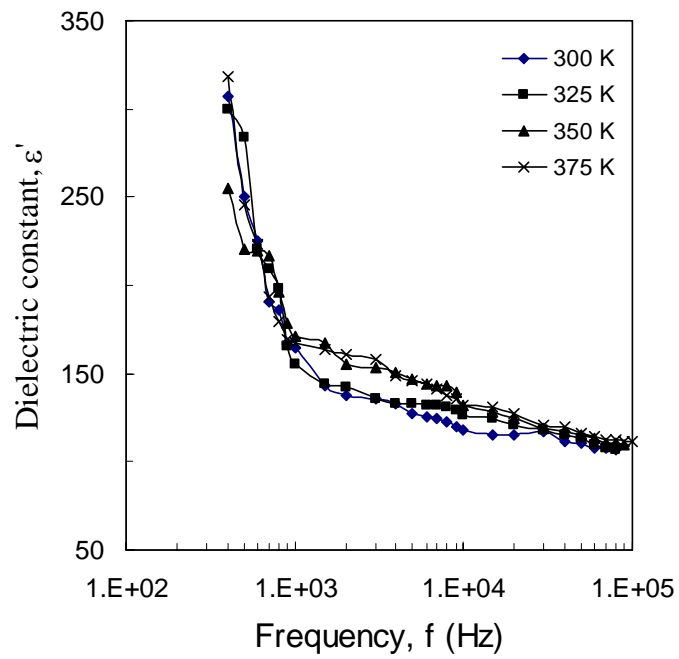


Figure 4.9 (b) Variation of dielectric constant with frequency for iPP/TiO₂ composite with 20 % TiO₂ at different temperatures.

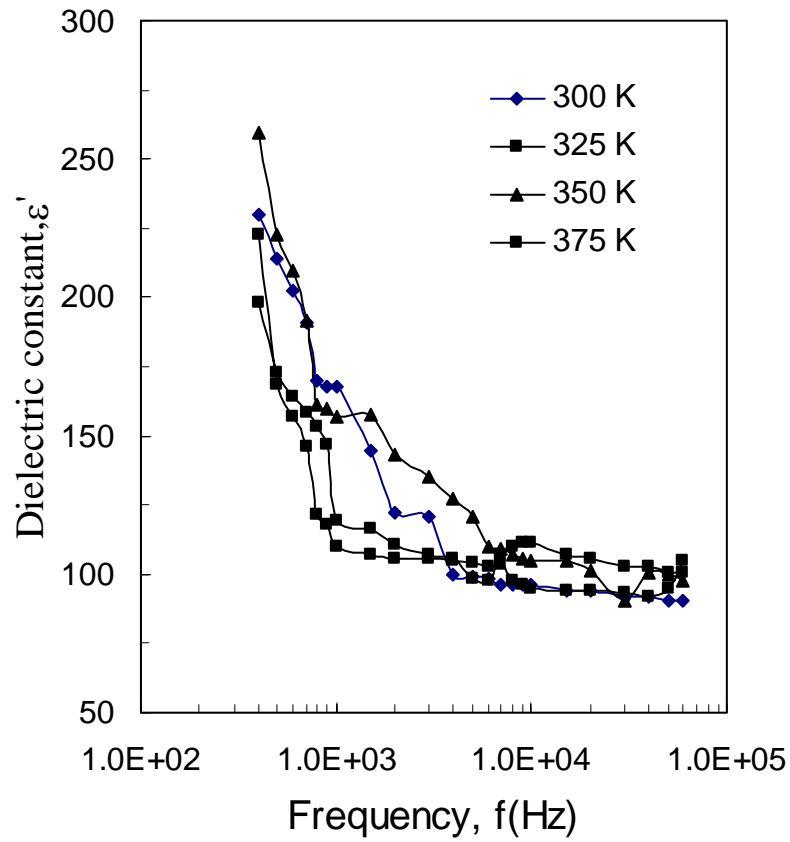


Figure 4.9 (c) Variation of dielectric constant with frequency for iPP/TiO₂ composite with 30 % TiO₂ at different temperatures.

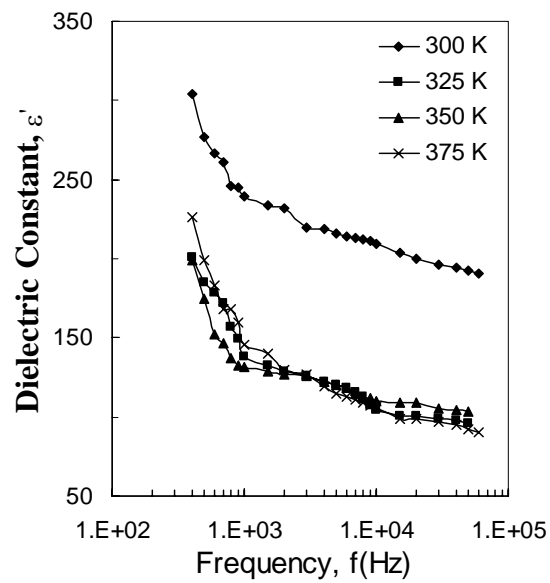


Figure 4.9(d) Variation of dielectric constant with frequency for iPP/TiO₂ composite with 40 % TiO₂ at different temperatures.

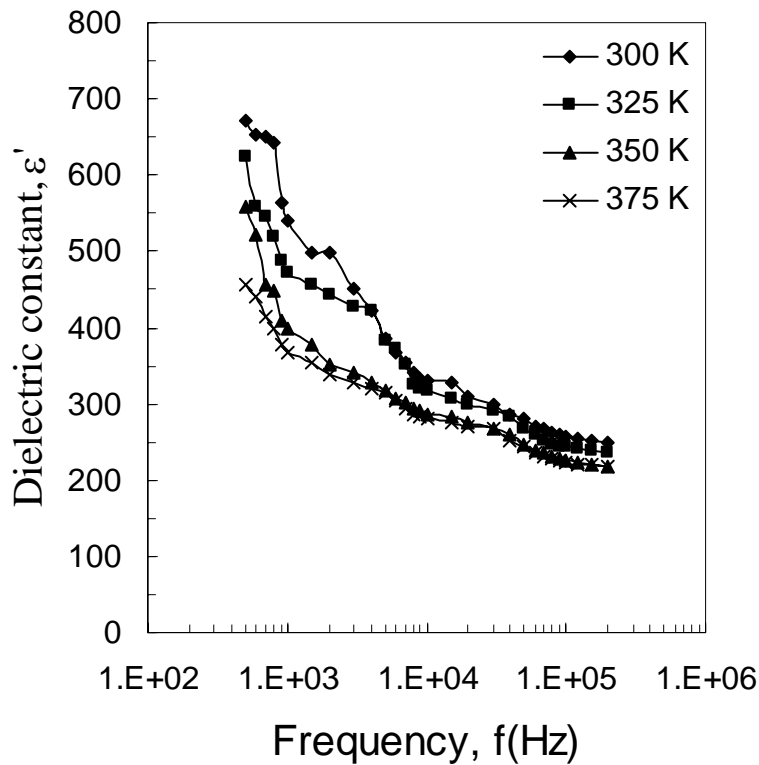


Figure 4.9(e) Variation of dielectric constant with frequency for iPP/TiO₂ composite with 50 % TiO₂ at different temperatures.

4.5.3 Variation of loss tangent with frequency and temperature

Figures 4.10(a)-4.10(d) show the variation of loss tangent with frequency at temperatures 300, 325, 350 and 375 K. It is observed that as the frequency increases the loss tangent increases and at a particular frequency the loss tangent attains a maximum value. After reaching the maximum, the loss tangent decreases with the increase in frequency. It is also observed that for a particular frequency, the loss tangent is higher at higher temperature. This low frequency relaxation peak indicates that the dielectric loss may be due to interfacial propagation in these composites.

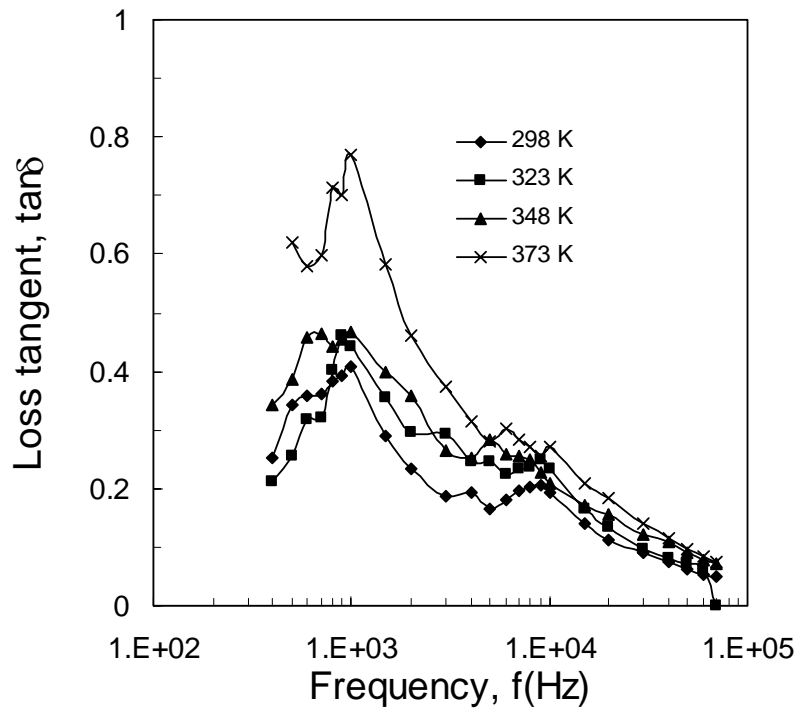


Figure 4.10 (a) Variation of loss tangent with frequency at different temperatures for iPP/TiO₂ composite with 10 wt % of TiO₂.

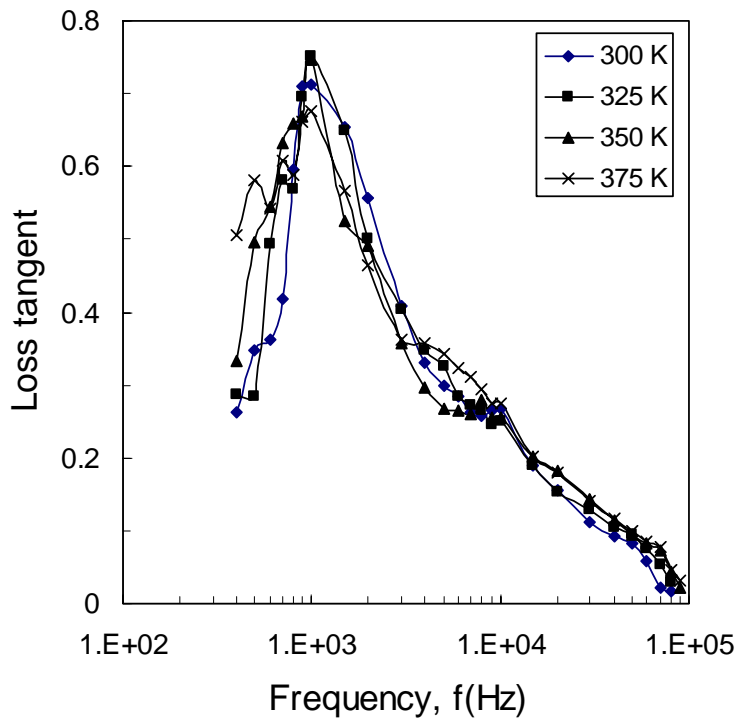


Figure 4.10 (b) Variation of loss tangent with frequency at different temperatures for iPP/TiO₂ composite with 20 wt % of TiO₂.

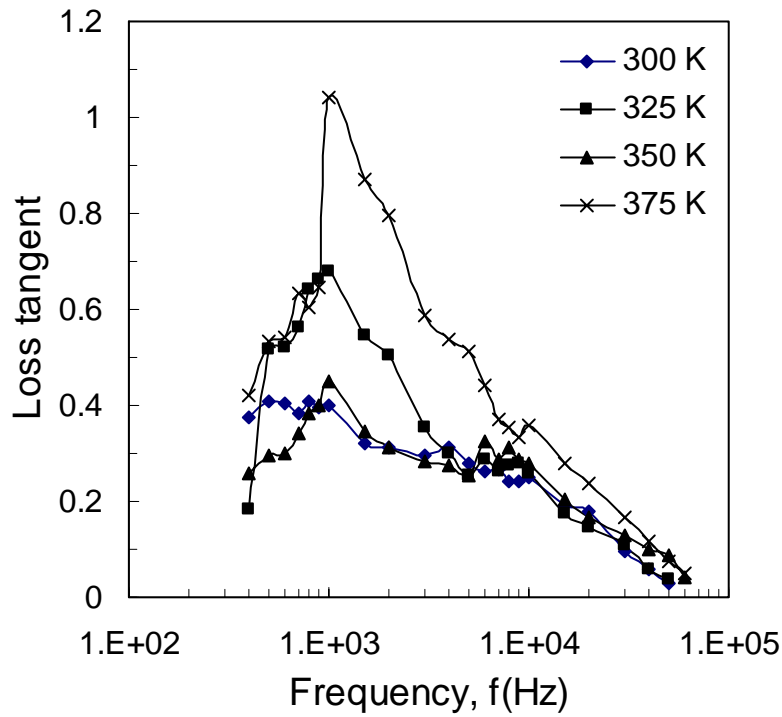


Figure 4.10 (c) Variation of loss tangent with frequency at different temperatures for iPP/TiO₂ composite with 30 wt % of TiO₂.

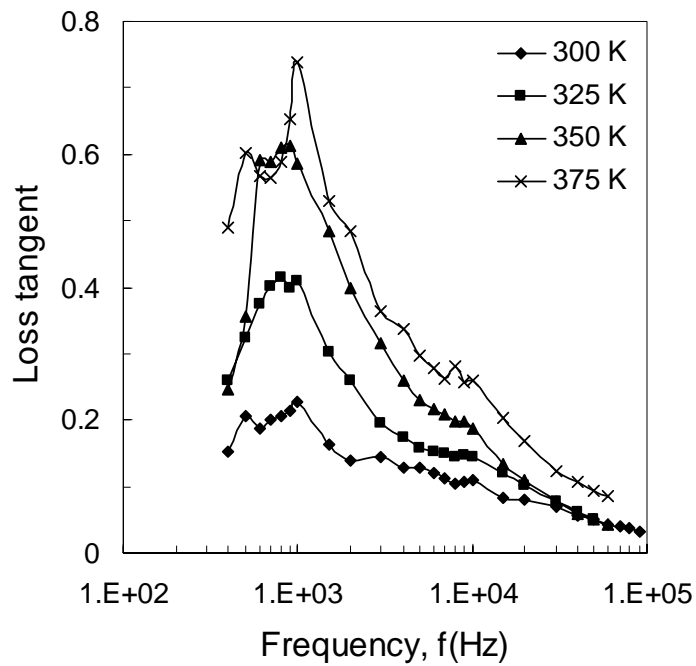


Figure 4.10 (d) Variation of loss tangent with frequency at different temperatures for iPP/TiO₂ composite with 40 wt % of TiO₂.

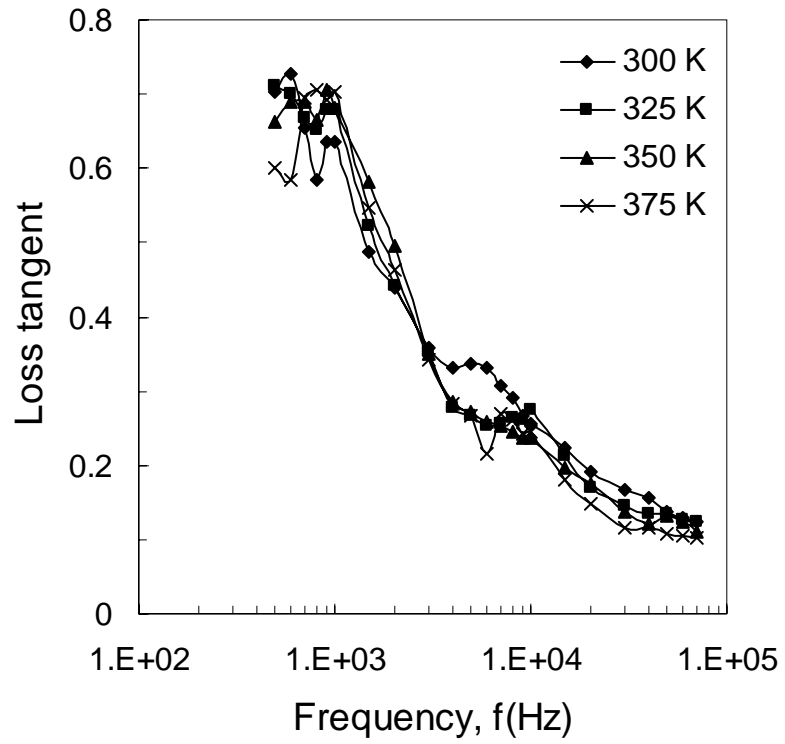


Figure 4.10 (e) Variation of loss tangent with frequency at different temperatures for iPP/TiO₂ composite with 50 wt % of TiO₂.

CHAPTER 5 CONCLUSIONS

5.1 Conclusions	77
5.2 Suggestions for future work	77
5.3 References	78

5.1 Conclusions

iPP-TiO₂ composites in four different weight of ratios have been studied with a view to investigate their SEM, mechanical properties, thermal properties and electrical properties. SEM micrographs provide us useful information about the microvoids or holes that increase in the composites with increasing the amount of filler. The reason of the presence of more holes may be for the development of interface around the particles due to their incompatibility with iPP matrix. These facts are confirmed by the generation of more holes in the SEM micrographs of 20 wt% TiO₂ loaded samples after fracture. The decrease of tensile strength and breaking strain is responsible for the decrease of crystallinity and crystallite size as well as for the increase in interfacial gap due to particle agglomeration in the composites. The decrease of microhardness and glass transition temperature with increasing filler content indicates that the composites are toughened after inclusion of titanium dioxide. In case of ac electrical measurement it is shown that AC conductivity increases with an increase of frequency and not much dependent on temperature. Dielectric constant decreases with increase in frequency but weakly dependent on temperature. From the variation between dielectric constant and filler content, it is observed that dielectric constant decreases with increase of filler loading. Loss tangent decreases with the increase of frequency but it increases with increase in temperature. Interfacial type relaxation is observed in these composites.

5.2 Suggestion for future work

The following investigations can be carried out for better understanding the behavior of these composites.

- Low concentration composition need to be studied.
- More structural investigations are necessary.
- Detail thermal analyses can be done to get more specific and quantative idea of thermal behavior of the composites.
- Detail DC electrical properties can be done to find the electrical applications.
- The dielectric constant, loss factor, and dielectric strength may be measured to find the electrical application of the materials.

5.3 References:

- [1] Liu, Z., Gilbert, M.J. “Structure and properties of talc-filled polypropylene: effect of phosphate coating”, *J. Appl. Polym. Sci.*, 59(7), 1087–1098, 1996.
- [2] Lee, Y.J., Manas-Zloczower, I, Feke, D.L., “Analysis of titanium dioxide agglomerate dispersion in linear low density polyethylene and resulting properties of compounds”, *Polym. Eng. Sci.*, 35(12), 1037–1045, 1995.
- [3] Mansour, S.H., Abd-El-Messieh, S.L., “Electrical and mechanical properties of some polymeric composites”, *J. Appl. Polym. Sci.*, 83, 1167–1180, 2002.
- [4] Luyt, A. S., Molefi, J. A., Krump, H., “Thermal, mechanical and electrical properties of copper powder filled low-density and linear low-density polyethylene composites”, *Polym. Degrad. Stab.*, 91,1629–1636, 2006.
- [5] Zhou, Y., Rangari, V., Mahfuz, H., Jeelani, S., Mallick, P. K., “Experimental study on thermal and mechanical behavior of polypropylene, talc/polypropylene and polypropylene/clay nanocomposites”, *Mater. Sci. Eng.*, 402, 109–117, 2005.
- [6] Wang, Y., Wang, J., ‘Shear yield behavior of calcium carbonate-filled polypropylene’, *Polym. Eng. Sci.*, 39(1), 190–198, 1999.
- [7] Lei, S.G., Hoa, S.V., “Ton-That MT. Effect of clay types on the processing and properties of polypropylene nanocomposites”, *Compos. Sci. Technol.*, 66, 1274–1279, 2006.
- [8] Semko, L. S., Kruchek, Ya. I., Shevlyakov, Yu. A., Gorbik, P. P., Oranskaya, E. I. *Inorg. Mat.* 43, 358–363, 2007.
- [9] Zhang, H., Zhang, Z., Park, H., Zhu, X., ‘Influence of surface- modified TiO₂ nanoparticles on fracture behavior of injection molded polypropylene’, *Front. Mater. Sci. China* 2(1), 9–15, 2008.
- [10] El-Midany, Ayman, A., Ibrahim, Suzan S., ‘The effect of mineral surface nature on the mechanical properties of mineral-filled polypropylene composites’, *Polym. Bull.*, 64, 387–399, 2010.
- [11] Guo, Z., Chen, J. Z., Xiaofei, W., Guoquan, S. L., ‘Assistant effect of nano-CaCO₃ particles on the dispersion of TiO₂ pigment in polypropylene composites’, *J. Mater. Sci.*, 39, 2891-2893, 2004.

- [12] Zohrab, A., Mohsen, A., Rahil H., Jaefar, N. R., 'Synthesis and Morphological Study of Nanoparticles Ag/TiO₂ Ceramic and Bactericidal Investigation of Polypropylene-Ag/TiO₂ Composite', *J. Inorg. Org. Polym.* 19, 322–327, 2009.
- [13] Wang, J. X., Yingpeng, Z.Z., Li J., Li, Chengwu, Z., Liquan X., Zhiqiang, X., Rui, Z., X., 'Photocatalytic degradation of organic dyes by Er³⁺:YAlO₃/TiO₂ composite under solar light', *Environ. Chem. Lett.* 8, 87–93, 2010.
- [14] Zhu, J., Yang, D., Geng, J., Chen, D., Jiang, Z., 'Synthesis and characterization of bamboo-like CdS/TiO₂ nanotubes composites with enhanced visible-light photocatalytic activity', *J. Nanopart. Res.* 10, 729–736, 2008.
- [15] Que, W., Zhou, Y., Lam, Y.L., Chan, Y.C., Kam, C.H., 'Preparation and characterizations of TiO₂/organically modified silane composite materials produced by the sol-gel method', *J. Sol-Gel Sci. Techn.* 20, 187–195, 2001.
- [16] Vasant Kumar, R., Raza, Ghulam, 'Photocatalytic disinfection of water with Ag–TiO₂ nanocrystalline composite', *Ionics.* 15, 579–587, 2009.
- [17] Cho, J., Schaab, S., Roether, J. A., Boccaccini, A. R., 'Nanostructured carbon nanotube/TiO₂ composite coatings using electrophoretic deposition (EPD)', *J. nanopart. Res.* 10, 99–105, 2008.
- [18] Moroz, N.A., Umapathy, H., Mohanty, P., 'Synthesis and Microstructure Evolution of Nano-Titania Doped Silicon Coatings', *JTTEE5* 19, 294–302, DOI: 10.1007/s11666-009-9443-x.
- [19] Lim, Y. V., Fan, H., Shen, Z., Huen, Kang, C. F., Feng, Y., Wang, S., 'Synthesis of silica supported titania nanocomposite in controllable phase content and morphology', *Appl. Phys. A* 95, 555–562, 2009.
- [20] Pendelyuk, Oksana I., Lisnycha, Tetyana V., Strelko, Volodymyr V., Kirillov, Sviatoslav A., 'Amorphous MnO₂–TiO₂ Composites as Sorbents for Sr²⁺ and UO₂²⁺', *Adsorption.* 11, 799–804, 2005.

- [21] Kokubo, Tadashi, Ueda, Takahiro, Kawashita, Masakazu, Gikan, Yuichi Ikuhara, Takaoka, H., Nakamura, Takashi., 'PET fiber fabrics modified with bioactive titanium oxide for bone substitutes', *J. Mater Sci. Mater. Med.* 19, 695–702, 2008.
- [22] Kim, H.-M., Miyaji, F., Kokubo, T., Nakamura, T., J., 'Bioactive polymeric nanocomposites for bone tissue engineering', *Biomed. Mater. Res.* 32, 409, 1996.
- [23] Miyazaki, T., Kim, H.-M., Miyaji, F., Kokubo, T., Nakamura, T., J. *Biomed.*, 'Bioactive tantalum metal prepared by NaOH treatment', *Mater. Res.* 50, 35, 2000.
- [24] Hou, Hongmei, Miyafuji, Hisashi, Kawamoto, Haruo, Saka, Shiro, 'Supercritically treated TiO₂ activated carbon composites for cleaning ammonia', *J. Wood Sci.* 52, 533–538, 2006.
- [25] He, Q., Yan, Liu, We, Feng, Yimin, Zhu, 'Structure and photochromic properties of molybdenum phosphoric acid/TiO₂ composite films', *Sci. China Ser B-Chem.* 52, 169-173, 2009.
- [26] Nazeri, A., Trzaskoma-Paulette, P.P., Bauer, D., 'Nanocrystalline ceria imparts better high- temperature protection', *J. Sol-Gel Sci.Techn.* 10, 317–331, 1997.
- [27] Bhuiyan, A. H., Mina, M. F., Seema, S., Khan, M. M., Rahman, M. J., Gafur, M. A., 'Structural, elastic and thermal properties of titanium dioxide filled isotactic polypropylene' *J Polym* 2010.
- [28] Yang J, Lin Y, Wang J, Lai M, Li J, Liu J, Tong X, Cheng H, 'Morphology thermal stability and dynamic mechanical properties of atactic polypropylene/carbon nano composites', *J Appl Polym Sci* 98:1087–1091, 2005.
- [29] Mubarak, Y.A., Abbadi, F.O., Tobgy, A.H., *J Appl Polym Sci*, 98, 1087–1091, 2005.
- [30] Mina MF, Haque MA, Bhuiyan MKH, Gafur MA, Tamba Y, Asano, 'Structural, elastic and Thermal Studies of TiO₂ filled isotactic polypropylene', *J Appl Polym Sci* 118, 312–319, 2010.
- [31] Chung MJ, Jang LW, Shim JH, Yoon JS, 'The effects of Chemical Bonding of nanoclay surface modifier and compatibilizer of microstructure development', *J Appl Polym Sci* 95, 307–311, 2005.

- [32] Brown J, Rhoney I, Pethrick RA, 'Epoxy resin based nanocomposites: 1. Diglycidylether of bisphenol A (DGEBA) with triethylenetetramine (TETA)', *Polym Int* 53, 2130–2137, 2004.
- [33] Wu DZ, Wang XD, Song YZ, Jin RG, *J Appl Polym Sci*, 92, 2714–2723, 2004.
- [34] Zhou RJ, Burkhart T, *J Mater Sci*, 45, 3016–3022, 2010
- [35] Wang SW, Yang W, Bao RY, Wang B, Xie BH, Yang MB, 'The enhanced nucleating ability of carbon nanotube-supported β -nucleating agent in isotactic polypropylene', *Colloid Polym Sci*, 288, 681–688, 2010.
- [36] Kumar, R. V., Koltypin, Y., Gedanken, A., 'Preparation and characterization of Nickel-polystyrene nanocomposite by ultrasound irradiation' *J. Appl. Polym. Sci.* 2002, 86(1):160.
- [37] Kumar, R. V., Koltypin Y., Cohen, Y. S., Cohen, Y., Aurbach, D., Palchik, O., et al 'preparation of amorphous magnetite nanoparticles in polyvinyl alcohol using ultrasonic radiation', *J. Mater. Chem.*, 10, 1125-7, 2000.
- [38] Saqan S, Zihlif AM, Ragosta G, *J Thermoplast Compos Mater*, 21, 457–467, 2008.
- [39] Thio YS, Argon AS, Cohen RE, Weinberg M, *Polymer* 43, 3661–3674, 2002
- [40] Wang Z, Hao W, Zhang Z, Cui Z, 'Structural, elastic and thermal properties of titanium dioxide filled isotactic polypropylene', *J Macromol Sci Part B* 47, 576–588, 2008.

INVESTIGATION OF THE MECHANICAL AND ELECTRICAL PROPERTIES OF
POLYPROPYLENE-TITANIUM OXIDE COMPOSITES.

Sharmin Seema

Student : M.Phil

Roll:040514017P

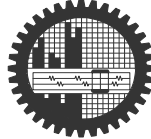
Session: April 2005



BUET

**DEPARTMENT OF PHYSICS
BANGLADESH UNIVERSITY OF ENGINEERING AND
TECHNOLOGY
DHAKA-1000, BANGLADESH**

**BANGLADESH UNIVERSITY OF ENGINEERING & TECHNOLOGY (BUET), DHAKA
DEPARTMENT OF PHYSICS**



BUET

Certification of Thesis Work

The thesis titled “INVESTIGATION OF THE MECHANICAL AND ELECTRICAL PROPERTIES OF POLYPROPYLENE-TITANIUM OXIDE COMPOSITES.” submitted by **Sharmin Seema**, Roll:040514017P, Session: April 2005, Registration No. : , has been accepted as satisfactory in partial fulfillment of the requirement for the degree of **MASTER of Philosophy (M. Phil.)** in **Physics** on **28 May, 2011**.

BOARD OF EXAMINERS

- (i) Professor Dr. Md. Abu Hashan Bhuiyan (Supervisor)
Chairman
Department of Physics, BUET, Dhaka 1000
- (ii) Head (Ex-Officio)
Member
Department of Physics, BUET, Dhaka 1000
- (iv) Prof. Dr. Nazma Zaman
Member
Department of Physics, BUET, Dhaka 1000
- (v)
- (vii) Member

Abstract

Table of Contents

Chapter 1	INTRODUCTION	Page
-----------	--------------	------

- 1.1 Introduction
- 1.2 Brief Reviews of Earlier Works
- 1.3 The aim of the Thesis
- 1.4 Thesis at a Glance
- References:

Chapter 2	POLYMERS, POLYPROPYLENE AND TiO ₂ COMPOSITES
-----------	--

- 2.1 Polymers**
 - 2.1.1 What is Polymer?**
 - 2.1.2 Classification of Polymers**
 - 2.1.3 Physical States of Polymer**
- 2.2 Polypropylene**
 - 2.2.1 Chemical and Physical Properties of Polypropylene**
 - 2.2.2 Electrical Properties**
 - 2.2.3 Mechanical Properties**
 - 2.2.4 Thermodynamic Properties**
 - 2.2.5 Application of Polypropylene**
- 2.3 Titanium dioxide (TiO₂)**
 - 2.3.1 Physical and Chemical Characteristics**
 - 2.3.2 Uses of TiO₂**
- 2.4 Composites**
 - 2.4.1 What are Composites?**
 - 2.4.2 Different types of Composite Materials**

2.5 Theory of Mechanical Properties of Composites

2.5.1 Concepts of Stress and Strain

2.5.2 Stress-strain Behaviour

2.5.3 Anelasticity

2.5.4 Tensile Properties

2.5.5 True Stress and Strain

2.5.6 Elongation

2.5.7 Hardness

Chapter 3 COMPOSITES

3.1 Raw Materials and sample preparation

3.2 Equipment for sample preparation

3.3 Sample preparation Procedure

3.4 Surface Morphology Testing

3.5 Method of Measuring of mechanical Properties

3.5.1 Equipment for mechanical testing

3.5.2 Micromechanical testing

3.5.3 Thermal testing

3.6 DC Electrical Measurements

3.6.1 Instruments

3.6.2 Methods

Chapter 4 THEORIES OF MECHANICAL PROPERTIES

4.1 Surface Morphology (SEM)

4.2 Mechanical properties (Tensile Properties)

4.3 Micromechanical Properties

4.4 Thermal Analysis

4.5 DC Electrical Studies (Current- Voltage Characteristics)

Chapter 5 AC ELECTRICAL PROPERTIES

Conclusions

5.1 Conclusions

5.2 Suggestion for future work

Chapter 6 THEORY OF THERMAL ANALYSIS

Chapter 7 EXPERIMENTAL DETAILS

(a) Raw materials used for sample preparation

(i) PP

(ii) TiO₂

(b) Sample preparation procedure

(c) Apparatus for sample preparation

(d) SEM

(e) Mechanical properties

(i) Equipment

(ii) Tensile Modulus

(iii) Flexural Modulus

(iv) Micromechanical testing

(v) Thermal analysis

Chapter 8 RESULTS AND DISCUSSIONS

Chapter 1: Introduction

Page

1.1 Introduction

1.2 Brief Reviews of Earlier Works

1.3 The aim of the Thesis

1.4 Thesis at a Glance

References:

Chapter 2 : Polymer, Plasma and Plasma Polymerization

2.1 Introduction

- 2.2 Polymer
 - 2.3. Plasma
 - 2.3.1 Applications of plasma
 - 2.4. Polymerization: Different Process
 - 2.5. Plasma Polymerization
 - 2.5.1 Fundamental aspects of Plasma Polymerization
 - 2.5.2 Pulsed Plasma Polymerization
 - 2.5.3 Advantages of Plasma Polymerization
 - 2.6. Different Types of Reactors
 - 2.7. Different Types of Glow Discharge
- References:

Chapter 3: Experimental Details

- 3.1 Introduction
- 3.2 Sample Preparation
- 3.3 Capacitively Coupled Plasma Polymerization Set up
- 3.4 Generation of glow discharge plasma
- 3.5 Film Thickness Measurement
- 3.6 Techniques applied for Characterization of thin films
 - 3.6.1 Scanning Electron Microscopy
 - 3.6.2 Differential Thermal Analysis
 - 3.6.3 Fourier Transform Infrared Analysis
 - 3.6.4 Ultra-Violet Spectroscopy
 - 3.6.5 Electrical Measurements
 - 3.6.5.1 DC electrical measurement
 - 3.6.5.2 AC electrical measurement

Chapter 4: Fourier Transform Infrared Spectroscopic Analysis

- 4.1 Introduction
 - 4.2 Theory of FTIR
 - 4.2.1 Introduction
 - 4.3 Instrumentation
 - 4.4 Experimental Procedure
 - 4.5 Results and Discussion
 - 4.5.1 FTIR analyses of VC, PPVC and heat treated PPVC
 - 4.6 Conclusions
- References

CHAPTER- 5 Ultraviolet Visible Spectroscopy

- 5.1 Introduction
- 5.2 Some aspects of UV-Vis spectroscopy
- 5.3 Beer –Lambert Law: The law of Absorption
- 5.4 Optical properties of Amorphous and Crystalline Materials
- 5.5 Experimental details
- 5.6 Instrumentation
- 5.7 Results and discussion

5.8 Conclusions

Chapter-6 Direct Current Electrical Properties

6.1 Introduction

6.2 Conductivity of thin films

6.2.1 Introduction

6.3 Direct Current Conduction mechanisms

6.3.1 Introduction

6.3.2 Charge transport process

6.3.3 Traps :

6.3.4 Mechanisms affecting the current transport

6.3.5 Poole-Frenkel effect

6.3.6 Schottky Mechanism: Image forces

6.3.7 Space Charge Limited Conduction

6.3.8 Tunneling

6.3.9 Thermally activated Conduction process

6.4 Results and discussion

6.4.1 Current density -Voltage characteristics

6.4.2 Conduction mechanism in PPVC thin films

6.4.3 Tunneling

6.4.4 Space Charge Limited Conduction (SCLC) process

6.4.5 Poole-Frenkel effect

6.4.6 Schottky mechanism

6.4.7 Temperature dependence of current density

7. Conclusions

Chapter-7 Alternating Current Electrical Properties

7.1 Introduction

7.2 Plasma polymers as dielectrics

7.2.1 Dielectric constant and Dielectric Loss

7.2.2 Polarization Mechanisms

7.2.3 Theory of dielectrics

7.2.4 Debye theory of dielectrics

7.2.5 Havriliak–Negami relaxation

7.2.6 Cole- Davidson equation

7.2.7 Cole –Cole equation

7.3 Experimental details

7.3.1 Experimental set up for plasma polymerization

7.3.2 Electrode preparation for electrical measurements

7.3.3 Alternating Current electrical measurement

7.4 Results and discussion

7.4.1 Variation of electrical conductivity with frequency and temperature

7.4.2 Variation of dielectric constant with frequency and temperature

7.4.3 Variation of dielectric loss tangent with frequency and temperature

7.4.4 Dependence of ϵ'' on ϵ' (Cole-Cole) plot

8. Conclusions

References:

Chapter- 8 Conclusions and suggestions for future work

8.1. Conclusions

8.2 Suggestions for future works

List of Figures

Chapter 1

None

Chapter 2

Figure 2.1 Polymer chain structure of one of the simplest and most common polymers: poly (ethylene)

Figure 2.2 Cascade process of ionization. Electrons are 'e⁻', neutral atoms 'o', and cations '+'.

Figure 2.3 Typical apparatus for CVD experiments, (a). Direct capacitively coupled parallel plate reactor, (b). Remote inductively coupled plasma.

Figure 2.4 Bell-jar reactor with parallel plate metal electrodes (internal reactor).

Figure 2.5 Electrodeless microwave reactor.

Figure 2.6 External electrode reactors.

Chapter 3

Figure 3.1 The chemical structure of vinylene carbonate (C₃H₂ O₃).

Figure 3.2 Schematic diagram of the plasma polymerization.

Figure 3.3 The Plasma polymerization Chamber

Figure 3.4 Interferometer arrangement for producing reflection Fizeau fringes of equal thickness.

Figure 3.5 Multiple Beam Interferometer

Figure 3.6 The Scanning Electron Microscope

Figure 3.7 The TG/DTA 6300

Figure 3.8 The FTIR spectrometer 8900

Figure 3.9 The UV- Visible spectrometer Shimadzu UV-1601

Figure 3.10 The Edward vacuum coating unit E306A

Figure 3.11 The electrode configuration for electrical measurements

Figure 3.12 A schematic circuit diagram of DC measurements

Figure 3.13 Arrangement of DC electrical measurement set-up

Figure 3.14 Arrangement of AC electrical measurement set-up

Chapter 4

Figure 4.1 Figure 4.1(a): The SEM micrographs of as deposited PPVC. (Mag. 10000 ×). (b) heat treated at 473 K for 1 hour (Mag. 10000 ×). (c) heat treated at 573 K for 1 hour (Mag. 10000 ×).

Figure 4.2 The DTA/TGA traces of as deposited PPVC.

Figure 4.3 Energy Levels in Molecules.

Figure 4.4 Infrared Spectroscopy Correlation diagram.

Figure 4.5 Stretching vibrations.

Figure 4.6 Bending vibrations.

Figure 4.7 The FTIR spectra of the VC, PPVC and PPVC heat treated at 473 and 573 K.

Chapter 5

Figure 5.1 The Electromagnetic Spectrum

Figure 5.2 Energy vs. Crystal momentum for a semiconductor with a direct band gap,

Figure 5.3 Vibrational and rotational energy levels of absorbing materials.

Figure 5.4 Different electronic transitions in the UV-Visible region.

Figure 5.5 Schematic diagram of a dual-beam UV-VIS spectrophotometer.

Figure 5.6 Variation of absorbance, ABS, with wavelength, λ for PPVC thin films of different thicknesses. (a) 200 nm (b) 175 nm (c) 150 nm (d) 125 nm

Figure 5.7 Plot of absorption co-efficient, α , as a function of photon energy, $h\nu$, for PPVC thin films of different thicknesses. (a) 200 nm (b) 175 nm (c) 150 nm (d) 125 nm

Figure 5.8 $(\alpha h\nu)^2$ vs. $h\nu$ curves for PPVC thin films of different thicknesses. (a) 200 nm (b) 175 nm (c) 150 nm (d) 125 nm

Figure 5.9 Variation of absorbance, ABS, with wavelength, λ for PPVC thin films at different thicknesses (Thickness: Monomer (1 cm), 80, 100, 150, 175, 200 nm)

Figure 5.10 Variation of absorbance, ABS, with wavelength, λ for PPVC thin films at different temperatures (Thickness: 200 nm)

Figure 5.11 Variation of Abs. coeff. with photon energy for PPVC thin films at different temperature (Thickness: 200 nm).

Figure 5.12 $(\alpha h\nu)^2$ vs. $h\nu$ curves for heat treated PPVC thin films of thicknesses (200nm)

Figure 5.13 Variation of absorption ABS, with wavelength, λ for PPVC thin films at different temperatures. (300 K, 473 K, 573 K. Thickness. 175 nm)

Figure 5.14 Variation of Abs. coeff. with photon energy for PPVC thin films at different temperature (300 K, 473 K, 573 K Thickness: 175 nm)

Figure 5.15 $(\alpha h\nu)^2$ vs. $h\nu$ curves for PPVC thin films at different temperature of thickness 175 nm

Figure 5.16 Variation of absorption ABS, with wavelength, λ for PPVC thin films at different temperatures. (300K, 473 K, 573 K. Thickness. 150 nm)

Figure 5.17 Variation of Abs. coeff. with photon energy for PPVC thin films at different temperature (Thickness: 150nm)

Figure 5.18 $(\alpha h\nu)^2$ vs. $h\nu$ curves for PPVC thin films at different temperature of thickness 150 nm

Figure 5.19 Variation of absorption ABS, with wavelength, λ for PPVC thin films at different temperatures. (300K, 473 K, 573 K. Thickness 100 nm)

Figure 5.20 Variation of Abs. coeff. with photon energy for PPVC thin films at different temperature (Thickness: 100 nm)

Chapter 6

Figure. 6.1 Schottky effect at a neutral contact

Figure. 6.2 Poole-Frenkel effect at a donor center.

Figure. 6.3 Energy diagram illustrating virtual cathode, cathode region, and anode region under space-charge-limited condition.

Figure. 6.4 Energy diagram showing shallow traps.

Figure. 6.5 SCLC I - V characteristic for an insulator containing shallow traps.

Figure 6.6 Variation of current density with applied voltage at different temperatures for PPVC thin film (thickness, $d=100$ nm).

Figure 6.7 Variation of current density with applied voltage at different temperatures for PPVC thin film (thickness, $d=130$ nm).

Figure 6.8 Variation of current density with applied voltage at different temperatures for PPVC thin film (thickness, $d=150$ nm).

Figure 6.9 Variation of current density with applied voltage at different temperatures for PPVC thin film (thickness, $d=200$ nm).

Figure 6.10 Variation of $\ln J$ with square root of applied voltage for PPVC thin film (thickness, $d=100$ nm) [Schottky plots].

Figure 6.11 Variation of $\ln J$ with square root of applied voltage for PPVC thin film (thickness, $d=130$ nm) [Schottky plots].

Figure 6.12 Variation of $\ln J$ with square root of applied voltage for PPVC thin film (thickness, $d=150$ nm) [Schottky plots].

Figure 6.13 Variation of $\ln J$ with square root of applied voltage for PPVC thin film (thickness, $d=200$ nm) [Schottky plots].

Figure 6.14 Variation of $\ln(J/T^2)$ with inverse absolute temperature for PPVC thin film (thickness, $d=100$ nm) [Richardson plots].

Figure 6.15 Variation of $\ln(J/T^2)$ with inverse absolute temperature for PPVC thin film (thickness, $d=130$ nm) [Richardson plots].

Figure 6.16 Variation of $\ln(J/T^2)$ with inverse absolute temperature for PPVC thin film (thickness, $d=150$ nm) [Richardson plots].

Figure 6.17 Variation of $\ln(J/T^2)$ with inverse absolute temperature for PPVC thin film (thickness, $d=200$ nm) [Richardson plots]

Figure 6.18 Fowler –Nordheim plots. (Thickness. 100 nm)

Figure 6.19 Fowler –Nordheim plots. (Thickness. 130 nm)

Figure 6.20 Fowler –Nordheim plots. (Thickness. 150 nm)

Figure 6.21 Fowler –Nordheim plots. (Thickness. 200 nm)

Chapter 7

Fig. 7.1 A dielectric permittivity spectrum over a wide range of frequencies. ϵ' and ϵ'' denote the real and the imaginary part of the permittivity, respectively

Fig: 7.2 Variation of ac conductivity with frequency at different temperature (film thickness, 100 nm).

Fig: 7.3 Variation of ac conductivity with frequency at different temperature (film thickness, 130 nm).

Fig: 7.4 Variation of ac conductivity with frequency at different temperature (film thickness, 150 nm).

Fig: 7.5 Variation of ac conductivity with frequency at different temperature (film thickness, 200 nm).

Fig. 7.6 Variation of ac conductivity with inverse absolute temperature at different frequency. (Thickness: 75 nm)

Fig. 7.7 Variation of ac conductivity with inverse absolute temperature at different frequency. (Thickness: 100 nm)

Fig. 7.8 Variation of ac conductivity with inverse absolute temperature at different frequency. (Thickness: 130 nm)

Fig. 7.9 Variation of ac conductivity with inverse absolute temperature at different frequency. (Thickness: 150 nm)

Fig. 7.10 Variation of ac conductivity with inverse absolute temperature at different frequency. (Thickness: 200 nm)

Fig. 7.11 Dielectric constant, ϵ as a function of frequency of the PPVC thin films of different thickness at room temperatures

Fig. 7.12 Dielectric constant, ϵ as a function of frequency of the PPVC thin films of thickness 100 nm at different temperatures

Fig. 7.13 Dielectric constant, ϵ as a function of frequency of the PPVC thin films of thickness 130 nm at different temperatures

Fig. 7.14 Dielectric constant, ϵ as a function of frequency of the PPVC thin films of thickness 150 nm at different temperatures

Fig. 7.15 Dielectric constant, ϵ as a function of frequency of the PPVC thin films of thickness 200 nm at different temperatures.

Fig. 7.16 Dielectric constant, ϵ' as a function of frequency of as deposited PPVC thin films of thickness 100 nm at different temperatures.

Fig. 7.17 Dielectric constant, ϵ' as a function of frequency of the PPVC thin films of thickness 100 nm at different temperatures after 70 days.

Fig. 7.18 Dielectric constant, ϵ as a function of temperature of the PPVC thin film of thickness 100 nm at different frequencies.

Fig. 7.19 Dielectric constant, ϵ as a function of temperature of the PPVC thin film of thickness 130 nm at different frequencies

Fig. 7.20 Dielectric constant, ϵ' as a function of temperature of the PPVC thin film of thickness 150 nm at different frequencies.

Fig. 7.21 Dielectric constant, ϵ as a function of temperature of the PPVC thin film of thickness 200 nm at different frequencies

Fig. 7.22 Dielectric loss tangent *with* frequency at different temperatures (100 nm)

Fig. 7.23 Dielectric loss tangent *with* frequency at different temperatures (130 nm)

Fig. 7.24 Dielectric loss tangent *with* frequency at different temperatures (150 nm)

Fig. 7.25 Dielectric loss tangent *with* frequency at different temperatures (200 nm)

LIST OF TABLES

Chapter 1

None

Chapter 2

None